**Università Roma Tre**

**Facoltà di Scienze Matematiche Fisiche e Naturali**

**Dipartimento di Scienze Geologiche**

**Dottorato di Ricerca in Geodinamica**

**XX Ciclo**

# Basalt/crust time-dependent interaction. Major and trace element behaviour in the resulting melts.

**Phd Student**

**Dott. Silvio Mollo**

**Tutor**

**Prof. Daniela Dolfi**

**Co-Tutor**

**Dott. Piergiorgio Scarlato**

# INDEX

# 1 - Introduction

Chemical variability of magmas outcropping world wide has been the focal point of petrological and geochemical studies since the first decade of the past century. Even if major processes have been clearly documented and actually accepted, a simple modelling cannot fully explain the chemical peculiarities of many magmatic products. The Italian Plio-Quaternary magmas constitute an example of the complex role played by the multiple processes invoked to explain geochemical, isotopic, and, at minor extent, major elements characters not consistent with simple models.

The serial characters of the Italian magmas span most of the world domain (Peccerillo, 2005 and references therein), reflecting the complex geodynamic setting of the peri-Tyrrhenian margin, dominated by the eastward migration of Tyrrhenian-Appennines subduction system, and by the related back-arc extension due to gravitational sinking of subducted Ionian lithosphere (Doglioni, 1991; Ferrari & Manetti, 1993; Faccenna et al., 1997; Carminati et al., 1998). Even for the most primitive compositions, four different mantle types, further metasomatized at various extent by variable crustal materials have been inferred mainly on geochemical and isotopic bases (Beccaluva et al., 1991; Serri et al., 1993; Lavecchia & Stoppa, 1996; Peccerillo, 1999; Lustrino et al., 2000; Castorina et al., 2000; Peccerillo & Lustrino, 2005). To complicate the picture, multiple interactions with crustal materials during the ascent of the parental melts, are often introduced to account for differences among the more or less evolved melts, even pertaining to same series.

Apart metasomatism of the source material, whatever the metasomatizing process could have occurred, evidences of mantle-magmas/crust interaction have been widely (and sometimes not univocally) documented. For example the chemical compositions of the most primitive melts erupted during the Plio-Quaternary in Sardinia suggest a magma generation from an OIB-type source contaminated by slab-derived components (Beccaluva et al., 1989); alternatively, it is suggested by Rutter (1987) that high K values and higher $^{87}Sr/^{86}Sr$ ratios (range 0.704-0.705) could have been acquired by a typical oceanic OIB-magmas assimilating upper crustal rocks. To explain the trace element variations of the Aeolian magmatism,

magma-crust interactions (e.g. AFC, Assimilation Fractional Crystallization; AEC, Assimilation Equilibrium Crystallization; RAFC, Refilling Assimilation Fractional Crystallization; RTFA, Refilling Tapping Fractionation Assimilation; etc.) has been frequently invoked by authors (Ellam & Harmon, 1990; Santo et al., 2004; Peccerillo et al., 2004; Frezzotti et al., 2003, Francalanci et al., 2005). Contamination at crustal levels has been proposed for the ultrapotassic magmas of the Central Appennine zone (Peccerillo, 1988) and recently assimilation of carbonaceous sediments has been documented for the Alban Hills magmatism (Dallai et al., 2004; Freda et al., 2006; Gaeta et al., 2006).

Contamination of a mantle magma by crustal materials concerns different topics, first of all the estimate of the heat amount involved in the assimilation process. The heat can be supplied or required by the hot magma according to exo- or endo-thermic reactions but a quantitative approach is very complicate because, while assimilating, the original magma behaves as an open system, exchanging elements with the surrounding rocks. Even if a theoretical approach has been proposed by Ghiorso (1985), lack of experimental data prevents its successful application to magmatic systems. Despite such big "inconvenient", it is now widely believed that hot mantle derived melts induce melting at the base of the crust and that mafic magmas frequently intrude silicic magma reservoirs within the crust. The density and viscosity differences between two chemically distinct contacting melts may be too large to allow mixing, and is still unclear under what conditions mingling (i.e. mechanical mixing) takes place and to what scale intimacy of melts is achieved before diffusion becomes the dominant homogenization process.

Mixing between mantle derived mafic melts and crustal derived, has been the topic of numerous studies (Taylor, 1980; De Paolo, 1981; Grove et al., 1988; Hildreth & Moorbath, 1988) and the current understanding reflects contributions from a large diversity of geological disciplines including field research, geochemical modelling, fluid mechanics and heat transfer studies, and experimental petrology.

The experimental approach has been mainly focused on the interaction between acid and mafic compositions (Yoder, 1973; Aliber & Carron, 1980; Watson, 1982; Watson & Jurewicz, 1984; Koyaguchi, 1989; Johnston & Wyllie, 1988; Wyllie et al., 1989; Van der Laan & Wyllie, 1993; Patino Douce, 1995)

trying to define the chemistries of the obtained hybrid melts or to punctualize diffusion processes. Results evidence variable diffusion rates for different elements and a wide spectrum of possible hybridized melts.

In the present thesis are experimentally investigated the effects of time on the rate and changes in the processes affecting the composition of a basaltic melt and the adjoining liquid and minerals of the crustal domain, with particular attention to the trace elements behaviour. Experimental temperature were kept high, while experiment durations were no longer than 8 h, in the attempt to simulate the process occurring in a large reservoir with a slow advancing crystallization front.

Two different crustal materials, separately coupled with the chosen basalt, have been used. Experimental pressures were in the range of the individuated stability fields for the two chosen crustal paragenesis.

Results evidence that chemical variations in the basalt domain are controlled by diffusion process at the contact with the more silicic liquid, whereas a complex interplay between diffusion, progressive melting of the crustal material, and crystallization reactions is reflected in the coupled experiments with the more mafic composition.

# 2 - Starting materials, experimental and analytical procedures

## *2.1 Starting materials and compositions*

A meta-anorthosite (MK72), a metapelite (VA38) and a calc-alkaline basalt (PF1) have been chosen for the experiments. Bulk analyses are reported in table 2.1.1.

MK72 comes from an exposed deep crustal section of the Pan-African belt (Tanzania), and represents the lowermost part of a continuous profile through the continental basement (Appel et al., 1998; Coolen, 1980; Muhongo & Lenoir, 1994). According to these authors, its P-T stability field is in the range of 0.8-1.0 GPa and 900 °C. The meta-anorthosite is a banded fine-grained rock. Layers (ranging from 2 to 7 mm in thickness) of granoblastic plagioclase (plg) are sub-parallel and alternate with layers (1 to 2 mm wide) of mixed phlogopite (phl), garnet (grt), hornblende (hbl), ilmenite (il), scapolite (sc) and occasional apatite (ap). Plagioclase is the major constituent of this metabasic rock (80 vol%) and displays a homogeneous composition ($An_{40}$).

VA38 comes from the Gennargentu Intrusive Complex of Sardinia (Italy). This rock represents the uppermost part of a continental crust and it has been well characterized in a previous unpublished Phd-thesis (Misiti, 2004), as the result of contact metamorphism produced by a quartz-dioritic intrusion into a Cambro-Ordovician pelitic sequences. The rock is a coarse-grained schist with layerings of felsic and mafic minerals. Grained quartz (q) is the most abundant phase (70 vol%) and muscovite (mus) + biotite (bt) + chlorite (chl) + sillimanite (sil) and magnetite (mt) occur in lepidoblastic beds and their modal percents are 25, 4 and 1 vol% respectively. To establish the P-T stability conditions we applied the quantitative petrogenetic grid for pelitic schists in the system KFMASH proposed by Spear & Cheney (1989), obtaining an interval of 0.4-0.5 GPa and 550-650 °C.

The basaltic rock is a poorly crystallized scoria product from Panarea Island (PF1). Intratelluric phases are represented by olivine, plagioclase, ±clinopyroxene.

The two crustal rocks were finely powdered in a agate mortar under acetone and dried at 110 °C before use, thus preserving the original amount of the

linked volatiles. In VA38 volatiles are mostly represented by $H_2O$. Very low amounts of chlorine, analyzed in the micas (<0.5 wt%) do not significantly change the volatile bulk composition accounting for the modal amount of the phyllosilicates.

Sulphur in the scapolite and fluorine in mica and amphibole, from MK72, could significantly contribute to the wt% of LOI, but their relative influence on melting is beyond the scope of this research and they were not accounted for.

Basalt clear glass, obtained from the natural sample at atmospheric pressure, was finely ground and small amounts of water (~1 wt%) were added to each run portion to restore the original content. Glass composition is reported in table 2.1.1. Oxide values overlap the bulk analysis and Fe or alkalies loss are not detected. Glass starting material was preferred to avoid interferences between original crystals and the eventually new-formed at the experimental conditions.

*Table 2.1.1. Bulk compositions of PF1, VA38, and MK72 starting materials and EPM analysis of PF1 glass. Bulk compositions have been determined by lithium metaborate/tetraborate fusion ICP analysis in Activation Laboratories Ltd (ACTLABS), Ontario, Canada. EPM analysis of PF1 glass is the average of 10 analytical spots.*

| wt% | PF1 glass | σ | PF1 bulk | σ | VA38 bulk | σ | MK72 bulk | σ |
|---|---|---|---|---|---|---|---|---|
| $SiO_2$ | 52.24 | 1.04 | 52.23 | 0.52 | 77.85 | 0.76 | 52.78 | 0.52 |
| $TiO_2$ | 0.58 | 0.02 | 0.57 | 0.01 | 0.60 | 0.01 | 0.84 | 0.01 |
| $Al_2O_3$ | 16.78 | 0.50 | 16.74 | 0.17 | 14.80 | 0.15 | 25.12 | 0.25 |
| FeO | 9.36 | 0.28 | 9.39 | 0.09 | 3.57 | 0.03 | 4.11 | 0.05 |
| MnO | 0.17 | 0.01 | 0.18 | - | 0.10 | - | 0.08 | - |
| MgO | 7.13 | 0.21 | 7.12 | 0.07 | 0.82 | 0.01 | 1.88 | 0.02 |
| CaO | 10.95 | 0.33 | 10.95 | 0.11 | 0.17 | - | 9.27 | 0.09 |
| $Na_2O$ | 1.81 | 0.05 | 1.83 | 0.02 | 0.20 | - | 5.15 | 0.05 |
| $K_2O$ | 0.85 | 0.03 | 0.86 | 0.01 | 1.76 | 0.02 | 0.57 | 0.01 |
| $P_2O_5$ | 0.13 | - | 0.13 | - | 0.14 | - | 0.18 | - |
| Total | 100.00 | | 100.00 | | 100.00 | | 100.00 | |
| Total* | 99.95 | | 99.08 | | 98.00 | | 99.31 | |
| LOI | | | 0.92 | | 2.00 | | 0.69 | |

*original total of the analysis

*2.2 Experimental procedures*

The experiments were prepared by loading 50 mg of PF1 glass-powder, doped with about 1 wt% of deionized water added by a micro-syringe, in the Pt-capsules (3.0 mm outer-diameter). The powder was tightly pressed at the bottom of the capsules to ensure a sharp interface between the underling and overlying compositions. The same amount of MK72 or VA38 was then added and the capsules were welded shut.

Optical analysis of previous experiments, not reported in the following chapters, suggested to run simultaneously each coupled-material capsule, with a second containing only the crustal sample. This procedure was reputed necessary to supervise the progressive melting of MK72 with run duration, whose chemistry overlaps the interaction process.

In all runs the basaltic material was below the crustal one and the two powders were separated by a sharp interface.

PF1 glass was prepared at the Dipartimento di Scienze Geologiche (Università di Roma Tre) in a Deltech DT-31 atmospheric pressure vertical rapid-quench furnace. Oxygen fugacity (NNO) was buffered by a CO-$CO_2$ gas mixture, controlled by a $SIRO_2$ solid zirconia electrolyte oxygen sensor. The oxygen sensor and internal thermocouple ($Pt_{87}Rh_{13}$-Pt, type R) are located at about 5 mm from the sample in the central part of the furnace which hot spot is about 4.5 cm long. The thermocouple was calibrated against the melting point of gold and is estimated to be accurate within ±3 °C. PF1, loaded in a Fe-presaturated Pt-capsules (5 mm outer diameter), was heated at 1400 °C, held at temperature for 20 minutes and rapidly quenched by dropping the sample into a water bath at the bottom of the furnace.

High pressure experiments were carried out at HP-HT Laboratory of Experimental Volcanology and Geophysics (Istituto Nazionale di Geofisica e Vulcanologia, Roma) in a solid-medium ¾ inch end-load piston-cylinder apparatus which ensures an isobaric quench with an initial quench rate of 2000 °C/min. The apparatus was calibrated for pressure and temperature as described by Bohlen (1984). Temperature was controlled by a factory calibrated $W_{95}Re_5$-$W_{74}Re_{26}$ thermocouple and held within 3 °C of the experimental temperature; gradient along the capsules was less than 10 °C according to that measured by

authors in the same experimental apparatus and conditions (Hudon et al., 1994). Capsules were positioned either into 19.1 mm long NaCl-crushable alumina-pyrex assembly.

Furnace assemblies consisted on an outer NaCl cylinder with inside a high-purity graphite furnace tube, surrounded by a pyrex glass sleeve. The capsules, 10 mm long, were inserted vertically into holes drilled in a solid MgO rods. The rods were then loaded into the graphite furnace tube. Care was taken to ensure that the centre of the capsules coincided with the centre of the hot-spot (10 mm length) of the furnace and with the position of the thermocouple. NaCl-crushable alumina-pyrophillite-pyrex assembly were adopted for samples with free-water added (Freda et al., 2001). After each experiment the position of the thermocouple relative to the capsules and the central hot-spot of the furnace was checked. Oxygen fugacity was not experimental buffered, but was imposed by these cell assemblies to NNO+2. This value has been obtained, adopting the Kress & Carmichael (1988) model knowing temperature, pressure and the $Fe^{+3}$ and $Fe^{+2}$ amounts, obtained by Mossbauer spectrometrical analyses on a PF1 test sample, run at the same P, T, and water condition as the other experiments. The estimated oxygen fugacity value is in agreement with those measured by Kushiro (1990) and Kawamoto and Hirose (1994) in hydrous and anhydrous melting experiments carried out in the same furnace assembly. They loaded different primitive compositions in Pt-capsules and determined oxygen fugacity values spanning from NNO+1.5 to NNO+2.

Samples were first pressurized at room temperature to the experimental pressure condition and then heated to the target temperature. Pressure was electronically maintained within ±0.02 GPa of working pressure. The quenched capsules were mounted horizontally in epoxy in brass tubes and they were then grounded and polished to expose a vertical slice of the capsule in its original position, for examination in reflected light and punctual analyses.

*2.3 Analytical techniques*

Major element analyses of the experimental products were performed at the CNR-Istituto di Geologia Ambientale e Geoingegneria (Rome, Italy) with a EPMA (Electron Probe Micro Analysis) Cameca SX50 equipped with five wavelength-dispersive spectrometers using 15 kV accelerating voltage, 15 nA beam current, 10 μm beam diameter, and 20 s counting time. The following standards were used: wollastonite (Si and Ca), corundum (Al), diopside (Mg), andradite (Fe), rutile (Ti), orthoclase (K), jadeite (Na), barite (Ba, S), celestine (Sr), F-phlogopite (F), and metals (Cr and Mn). Ti and Ba contents were corrected for the overlap of the Ti $K_\alpha$ and Ba $K_\alpha$ peaks.

Trace element analyses were performed at the at the CNR-IGG–Pavia with a LA-ICP-MS (Laser Ablation Inductively Coupled Plasma Mass Spectrometry) apparatus. The laser source consists of a Q-switched Nd:YAG laser (Brilliant, Quantel), whose fundamental emission in the near-IR region (1064 nm) is converted into 266 nm by two harmonic generators. Using mirrors, the laser beam is carried into a petrographic microscope, focused above the sample, and then projected onto it.

The ablated material is analyzed with a single-collector double-focusing sector-field ICP–MS (Element, Finnigan Mat, Bremen, Germany). The mass spectrometer alignment was initially performed using nebulization of standard solutions and then optimized for dry plasma with the laser probe. Fine alignment (optimum RF power and gas flows) is performed before every analytical session on the NIST 610 glass reference material by maximizing the signals of $^{139}La$ and $^{232}Th$, and monitoring the $ThO^+/Th^+$ ratio in order to estimate the formation of polyatomic oxides. Optimum average instrumental operating conditions are: RF power 800-900 W, cooling gas 12.08 l/min, sample gas 0.9-1.1 l/min, auxiliary gas 1.00 l/min and carrier gas 0.9-1.1 l/min. The 34 masses of petrological interest between $^{25}Mg$ and $^{238}U$ that were selected for analysis are reported in table 2.3.1.

As reported in table, the total scan-time of the 34 selected masses is about 700 ms, the settling time is about 340 ms, and hence the acquisition efficiency is estimated at about 50%. A typical analysis consists of acquiring one minute of background and one minute of ablated sample, thus approximately 170 sweeps are required. The mean integrated time for acquisition is about 0.9 s for each element.

A typical analytical run consists of 20 analyses in which the first and last two are standard materials. Data reduction is performed by means of the GLITTER® software (Macquarie Research Ltd., 2001) developed by Van Achterbergh et al. (1999).

Image analyses and chemical maps were performed at the HP-HT Laboratory of Experimental Volcanology and Geophysics (Istituto Nazionale di Geofisica e Vulcanologia, Roma) with a Jeol FE-SEM (Field Emission Scanning Electron Microscope) 6500F equipped with a EDS (Energy Dispersion microanalysis System).

Mössbauer spectroscopy was performed at Dipartimento di Scienze della Terra, Università Sapienza di Roma. Samples were prepared by pressing the powdered glass with an acrylic resin to obtain self-supporting absorbers with Fe thickness in the range 1–2 mg/cm$^2$. Spectra were collected at room temperature using a conventional spectrometer system operating in constant acceleration mode with a $^{57}$Co source of nominal 50 mCi in Rh matrix. Spectral data in the velocity range from -4 to 4 mm/s were recorded by a 512 multichannel analyser. After velocity calibration against a spectrum of high-purity $\alpha$-iron foil (25 μm thick), the raw data were folded to 256 channels. The spectra were fitted, assuming Lorentzian peak shape, using the fitting program Recoil 1.04. Reduced $\chi^2$ was used as a parameter to evaluate statistical best fit, and uncertainties were calculated using the covariance matrix. Errors are estimated at about ±0.02 mm/s for isomer shift, quadrupole splitting, and no more than ±3% for doublet areas.

Water contents were measured by FTIR (Fourier Transform Infrared Spectroscopy) from the 3500 cm$^{-1}$ absorption band adopting the absorption coefficient of Dixon et al. (1988) in the FTIR-Laboratory, at the University of Roma Tre (Rome, Italy). To determine water contents, doubly polished thin sections from experimental samples were analyzed using a Nicolet NicPlan microscope equipped with a KBr beam splitter and an MCT (Mercury, Cadmium, Telluride) nitrogen-cooled detector.

*Table 2.3.1. Acquisition list parameters for trace-element determinations.*

| Element | Mass (a.m.u.) | Settling time (ms) | Sample time (ms) | Samples per peak | Segment duration (ms) | Mass window (%) | Type of acquisition | Total time (ms) |
|---|---|---|---|---|---|---|---|---|
| Mg | 25 | 80 | 3 | 3 | 15 | 160 | Analog | 95 |
| Si | 29 | 2 | 1 | 8 | 14 | 160 | Analog | 16 |
| Ca | 43 | 33 | 1 | 9 | 11 | 110 | Both | 44 |
| Cs | 44 | 1 | 1 | 8 | 11 | 110 | Analog | 12 |
| Sc | 45 | 1 | 1 | 9 | 11 | 110 | Both | 12 |
| Ti | 49 | 1 | 1 | 9 | 11 | 110 | Both | 12 |
| V | 51 | 1 | 1 | 9 | 11 | 110 | Both | 12 |
| Cr | 53 | 1 | 1 | 9 | 11 | 110 | Both | 12 |
| Rb | 85 | 50 | 1 | 9 | 11 | 110 | Both | 61 |
| Sr | 88 | 1 | 1 | 9 | 11 | 110 | Both | 12 |
| Y | 89 | 1 | 1 | 9 | 11 | 110 | Both | 12 |
| Zr | 90 | 1 | 1 | 9 | 11 | 110 | Both | 12 |
| Nb | 93 | 1 | 1 | 9 | 11 | 110 | Both | 12 |
| Cs | 133 | 45 | 1 | 9 | 11 | 110 | Both | 56 |
| Ba | 137 | 1 | 1 | 9 | 11 | 110 | Both | 12 |
| La | 139 | 1 | 1 | 9 | 11 | 110 | Both | 12 |
| Ce | 140 | 1 | 1 | 9 | 11 | 110 | Both | 12 |
| Pr | 141 | 1 | 1 | 9 | 11 | 110 | Both | 12 |
| Nd | 146 | 1 | 1 | 9 | 11 | 110 | Both | 12 |
| Sm | 149 | 1 | 1 | 9 | 11 | 110 | Both | 12 |
| Eu | 151 | 1 | 1 | 9 | 11 | 110 | Both | 12 |
| Gd | 157 | 1 | 1 | 9 | 11 | 110 | Both | 12 |
| Tb | 159 | 1 | 1 | 9 | 11 | 110 | Both | 12 |
| Dy | 163 | 1 | 1 | 9 | 11 | 110 | Both | 12 |
| Ho | 165 | 30 | 1 | 9 | 11 | 110 | Both | 41 |
| Er | 167 | 1 | 1 | 9 | 11 | 110 | Both | 12 |
| Tm | 169 | 1 | 1 | 9 | 11 | 110 | Both | 12 |
| Yb | 173 | 1 | 1 | 9 | 11 | 110 | Both | 12 |
| Lu | 175 | 1 | 1 | 9 | 11 | 110 | Both | 12 |
| Hf | 177 | 1 | 1 | 9 | 11 | 110 | Both | 12 |
| Ta | 181 | 1 | 1 | 9 | 11 | 110 | Both | 12 |
| Pb | 208 | 37 | 1 | 9 | 11 | 110 | Both | 48 |
| Th | 232 | 1 | 1 | 9 | 11 | 110 | Both | 12 |
| U | 238 | 1 | 1 | 9 | 11 | 110 | Both | 12 |

## 3 - Basalt/meta-anorthosite interaction

Experimental configurations are summarized in table 3.1.
Run conditions were super liquidus for the basalt. However MELTS calculations (Ghiorso & Sack, 1995) performed at 0.8 GPa and $fO_2$=NNO+2 denote a liquidus at 1270 °C for the PF1 anhydrous composition, while such temperature is lowered by 30 °C upon addition of 1 wt% water.

Sub-liquidus experimental conditions for the meta-anorthosite are confirmed by MELTS and are not the consequence of the short run durations. MELTS gives a $T_{liq}$ at 1330 °C for a MK72 anhydrous starting material and a $T_{liq}$ at 1290 °C when 1 wt% of $H_2O$ is added; in both cases plagioclase is the liquidus phase, joined by a low-Ca pyroxene at 1195 °C, or by spinel at 1150 °C , respectively in absence or in presence of water.

*Table 3.1. Experimental conditions and configurations.*

| Run# | T (°C) | P (Gpa) | t (h) | $H_2O$* (wt%) | starting material | products |
|---|---|---|---|---|---|---|
| PC177 | 1200 | 0.8 | 1 | 1.0 | PF1/MK72 | g/plg+g |
| PC219 | 1200 | 0.8 | 2 | 0.9 | PF1/MK72 | g/plg+g |
| PC218 | 1200 | 0.8 | 4 | 1.1 | PF1/MK72 | g/plg+g |
| PC254 | 1200 | 0.8 | 8 | 0.8 | PF1/MK72 | g/plg+g |
| PC177 | 1200 | 0.8 | 1 | - | MK72 | plg+g |
| PC219 | 1200 | 0.8 | 2 | - | MK72 | plg+g |
| PC218 | 1200 | 0.8 | 4 | - | MK72 | plg+g |
| PC254 | 1200 | 0.8 | 8 | - | MK72 | plg+g |

*amount of added water to the basaltic composition

Products from the coupled experiments consist of a partially molten MK72 overlying a PF1 brown glass. Partially molten MK72 is the results of melting experiments with the anorthosite alone. At the contact of the two compositions a not fully regular interaction layer developed, probably as a consequence of deformation during the pressurization stage (fig. 3.1).

Details are reported in the following sessions.

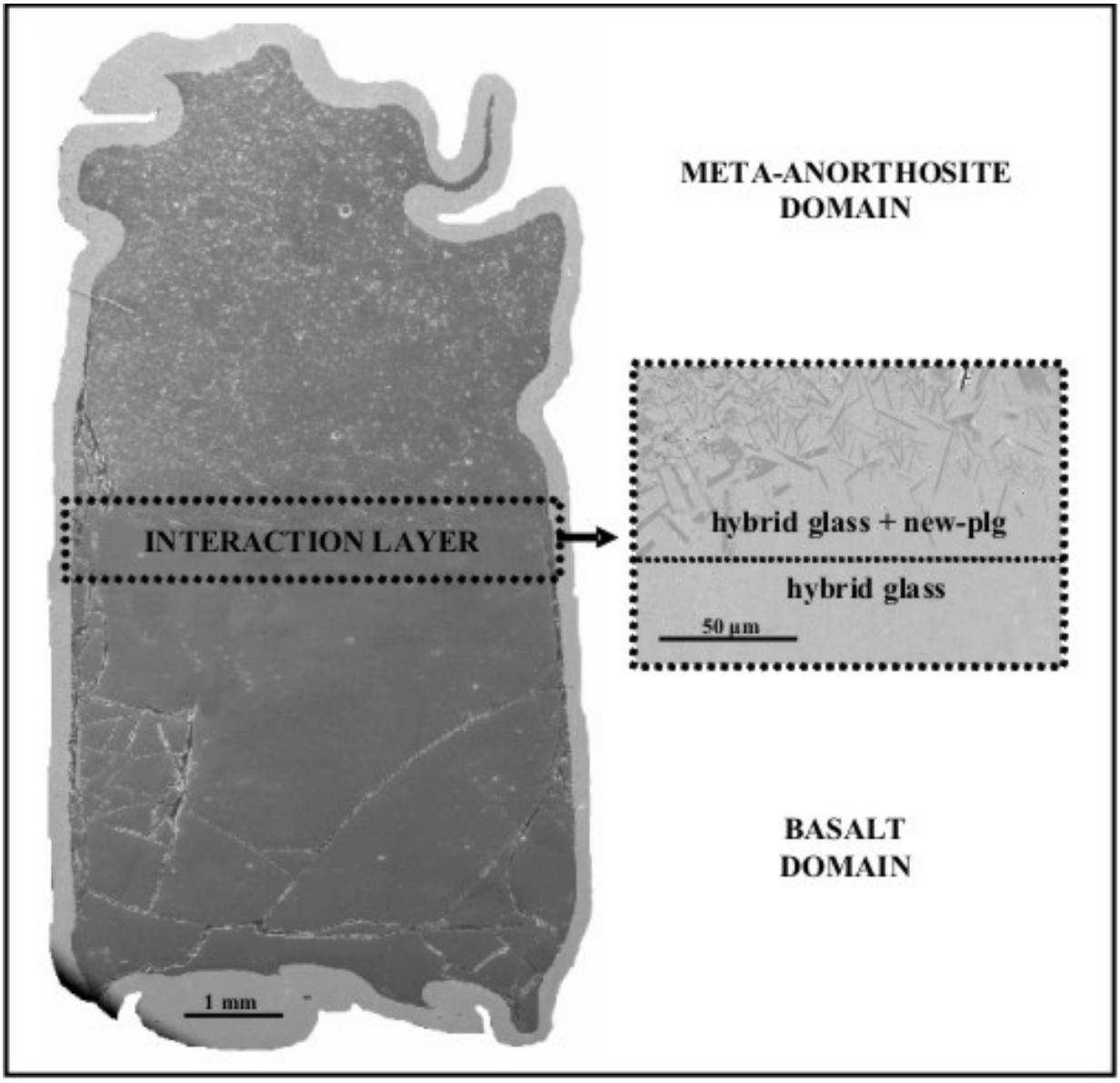


*Figure 3.1. FE-SEM backscattered electrons image of coupled experiments, after the 4h run. The basaltic melt (PF1) and partially molten granulite (MK72) occupy the bottom and the top of the capsule respectively. A detail of the interaction layer between PF1 and MK72 shows the occurrence of new-plg from the hybrid glass.*

### *3.1 Textural characters*

MK72 is partially melted and percent of melt increases with time, from ~45 vol% to ~60 vol%, as obtained through image analyses performed by FE-SEM chemical mapping.

In the 1 and 2 h runs, glass is present as small clear patches uniformly distributed (fig. 3.1.1a-b) within the investigated slide. Prolonged duration causes a disaggregation of the context with film of inter-granular liquid pervading the

syntherized powder (fig. 3.1.1c). Finally larger patches of melts are well developed after 8 h (fig. 3.1.1d).

Plagioclase is always the only residual mineral. A "like-porphyritic" texture develops with time, probably triggered by the not homogeneous grain-size of the starting material. Little grains are faster consumed in the melt, showing a decreasing average-size with time (fig. 3.1.1). On the contrary, larger, rounded grains are prone to preserve their dimensions as well as the original chemistry ($An_{44}$). Such grains are sieve textured showing a marginal selective resorption: a more calcic plagioclase mantles the crystals thus preventing the internal part from coming into contact with the liquid.

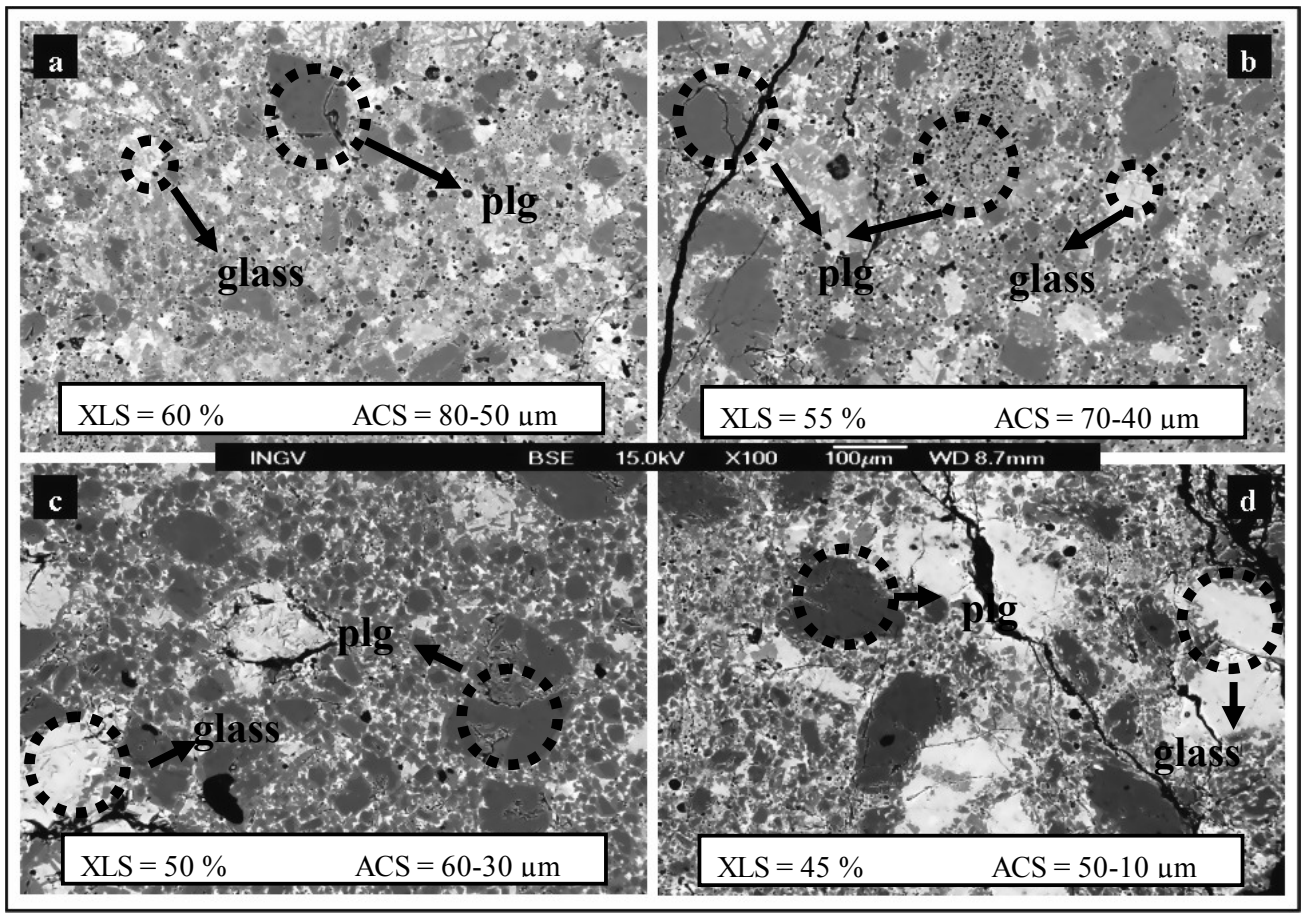


*Figure 3.1.1. MK72 plagioclase and glass distribution. a) 1 h run; b) 2 h run; c) 4 h run; d) 8 h run. XLS = volume percent of crystallization. ACS=average crystal size in µm.*

Such configuration slows down the melting process of large grains, for two main reasons: a) the reduced gradient among the chemical potentials of the An, Ab, Or, components in the coexisting solid and liquid phases, in the attempt to approach

equilibrium conditions; b) the closed system of binary type represented by the interior of the crystals, that as such exhibits much higher liquidus temperature than the multi-component liquid.

The interaction zone between MK72 and PF1, is characterized by a layer of clear glass shading to brown towards the basalt domain. Thickness of such layer does not consistently change with time, preserving an average value of 0.8 mm. In spite of such evenness, crystals of plagioclase nucleate and develop with time, at distance within ~400 μm from the MK72 side. Acicular (2×20 μm) crystals are present in the 1 and 2 h runs; they turn to a tabular shape (10×50 μm) after 4 and 8 h. Image analyses reveal an increasing crystallization from 5 vol% to 20 vol% within the experimental times (fig. 3.1.2a-b).

A uniform, brown glass, devoid of crystals constitutes the product of all the experiments on the PF1 portion of the capsule.

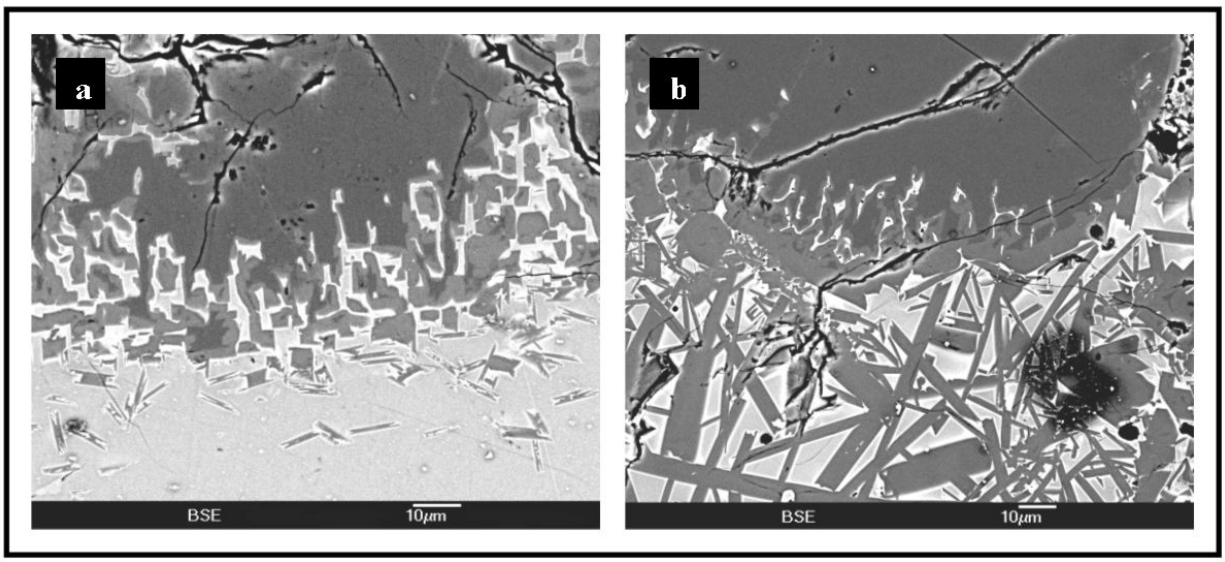


*Figure 3.1.2. Plagioclases at the contact and within the interaction layer between anorthosite and basalt compositions. On the top is evident a big sieve-textured residual crystal at the bordering zone. New crystallized plagioclases growing from the light, hybrid melt. a) 1 hour experiment. b) 8 hours experiment.*

### *3.2 Mineral chemistries*

In table 3.2.1 chemical analyses of restitic plagioclase are reported. Rim chemistries are from large, partially resorbed crystals. The core composition is homogeneous and strictly matches the original composition ($An_{44}$), whilst the rims change with time. According to selective melting, rims are An enriched with

respect to natural plagioclase which is stable at temperatures lower than the experimental. Sieve-texture accounts for a disequilibrium process; even if from our data it is not possible to determine the equilibrium composition a clear trend towards more An enriched terms is evidenced (fig. 3.2.1) with time. MELTS suggests an equilibrium composition of $An_{60}$-$Ab_{40}$ which should be attained after ~30 h run duration, according to a rough estimate based on the rate of the analyzed chemical variations. Enrichments in the An molecule are joined by a similar trend in Or content. Such feature clearly distinguishes resorbed from the new crystallized plagioclase (fig. 3.2.2).

*Table 3.2.1. Restitic plagioclase chemical compositions. Reported values are the average of 15 microprobe analyses. Plagioclase structural formulas based on 8 oxygens.*

| Run# | natural | | PC177 | | | | PC219 | | | | PC218 | | | | PC254 | | | |
|---|---|---|---|---|---|---|---|---|---|---|---|---|---|---|---|---|---|---|
| time (h) | plagioclase | | 1 | | | | 2 | | | | 4 | | | | 8 | | | |
| wt% | | σ | Core | σ | Rim | σ | Core | σ | Rim | σ | Core | σ | Rim | σ | Core | σ | Rim | σ |
| $SiO_2$ | 57.11 | 0.55 | 57.06 | 0.57 | 55.40 | 0.55 | 57.00 | 0.57 | 54.72 | 0.55 | 57.06 | 0.55 | 54.12 | 0.54 | 57.05 | 0.56 | 53.71 | 0.54 |
| $Al_2O_3$ | 27.03 | 0.25 | 27.04 | 0.27 | 28.02 | 0.28 | 27.04 | 0.25 | 28.34 | 0.28 | 27.04 | 0.27 | 28.65 | 0.28 | 27.04 | 0.27 | 29.10 | 0.29 |
| $Fe_2O_3$ | 0.20 | - | 0.24 | - | 0.33 | - | 0.24 | - | 0.50 | 0.09 | 0.23 | - | 0.62 | 0.10 | 0.25 | - | 0.40 | - |
| CaO | 9.11 | 0.08 | 9.11 | 0.09 | 10.40 | 0.10 | 9.20 | 0.08 | 10.88 | 0.13 | 9.11 | 0.10 | 11.33 | 0.11 | 9.13 | 0.09 | 11.70 | 0.12 |
| $Na_2O$ | 6.33 | 0.06 | 6.31 | 0.07 | 5.47 | 0.05 | 6.29 | 0.06 | 5.16 | 0.06 | 6.31 | 0.06 | 4.86 | 0.05 | 6.29 | 0.06 | 4.66 | 0.05 |
| $K_2O$ | 0.20 | - | 0.22 | - | 0.35 | - | 0.21 | - | 0.37 | - | 0.22 | - | 0.39 | - | 0.22 | - | 0.40 | - |
| Total | 99.98 | | 99.99 | | 99.96 | | 99.98 | | 99.97 | | 99.98 | | 99.97 | | 99.98 | | 99.97 | |
| | | | | | | | | | | | | | | | | | | |
| Si | 2.563 | | 2.561 | | 2.498 | | 2.559 | | 2.473 | | 2.561 | | 2.450 | | 2.561 | | 2.433 | |
| Al | 1.430 | | 1.431 | | 1.491 | | 1.431 | | 1.510 | | 1.431 | | 1.529 | | 1.431 | | 1.553 | |
| Fe | 0.007 | | 0.008 | | 0.011 | | 0.008 | | 0.017 | | 0.008 | | 0.021 | | 0.008 | | 0.014 | |
| Ca | 0.438 | | 0.438 | | 0.502 | | 0.443 | | 0.527 | | 0.438 | | 0.550 | | 0.439 | | 0.568 | |
| Na | 0.551 | | 0.549 | | 0.478 | | 0.548 | | 0.452 | | 0.549 | | 0.427 | | 0.547 | | 0.409 | |
| K | 0.011 | | 0.013 | | 0.020 | | 0.012 | | 0.021 | | 0.013 | | 0.023 | | 0.013 | | 0.023 | |
| | | | | | | | | | | | | | | | | | | |
| An | 43.80 | | 44.05 | | 50.22 | | 44.19 | | 52.67 | | 43.89 | | 55.03 | | 43.95 | | 56.77 | |
| Ab | 55.05 | | 54.30 | | 47.80 | | 55.10 | | 45.20 | | 54.80 | | 42.72 | | 54.79 | | 40.92 | |
| Or | 1.15 | | 1.29 | | 1.99 | | 1.28 | | 2.13 | | 1.31 | | 2.26 | | 1.26 | | 2.31 | |

In table 3.2.2. chemical analyses of the nucleated crystals are reported. No analyses have been obtained for the shortest run because of the dimensions of the crystals. Slightly different plagioclases have been accurately analyzed in the longer runs.

*3.2.2. Chemical variations of new-formed plagioclases. Mineral values are the average of 15 different analyses.*

| Run# | PC177 | | PC219 | | PC218 | |
|---|---|---|---|---|---|---|
| time (h) | 2 | | 4 | | 8 | |
| wt% | Neo-Plg | σ | Neo-Plg | σ | Neo-Plg | σ |
| $SiO_2$ | 52.05 | 0.52 | 52.10 | 0.50 | 52.20 | 0.53 |
| $Al_2O_3$ | 29.50 | 0.30 | 29.61 | 0.25 | 29.51 | 0.27 |
| $Fe_2O_3$ | 1.18 | 0.01 | 1.05 | 0.01 | 1.03 | 0.02 |
| CaO | 13.15 | 0.13 | 13.05 | 0.09 | 13.00 | 0.17 |
| $Na_2O$ | 3.85 | 0.04 | 3.90 | 0.07 | 4.00 | 0.05 |
| $K_2O$ | 0.25 | - | 0.24 | - | 0.24 | - |
| Total | 99.98 | | 99.95 | | 99.98 | |
| | | | | | | |
| Si | 2.372 | | 2.373 | | 2.377 | |
| Al | 1.585 | | 1.590 | | 1.584 | |
| Fe | 0.040 | | 0.036 | | 0.035 | |
| Ca | 0.642 | | 0.637 | | 0.634 | |
| Na | 0.340 | | 0.344 | | 0.353 | |
| K | 0.014 | | 0.014 | | 0.014 | |
| | | | | | | |
| An | 64.42 | | 64.00 | | 63.25 | |
| Ab | 34.14 | | 34.60 | | 35.30 | |
| Or | 1.45 | | 1.45 | | 1.39 | |

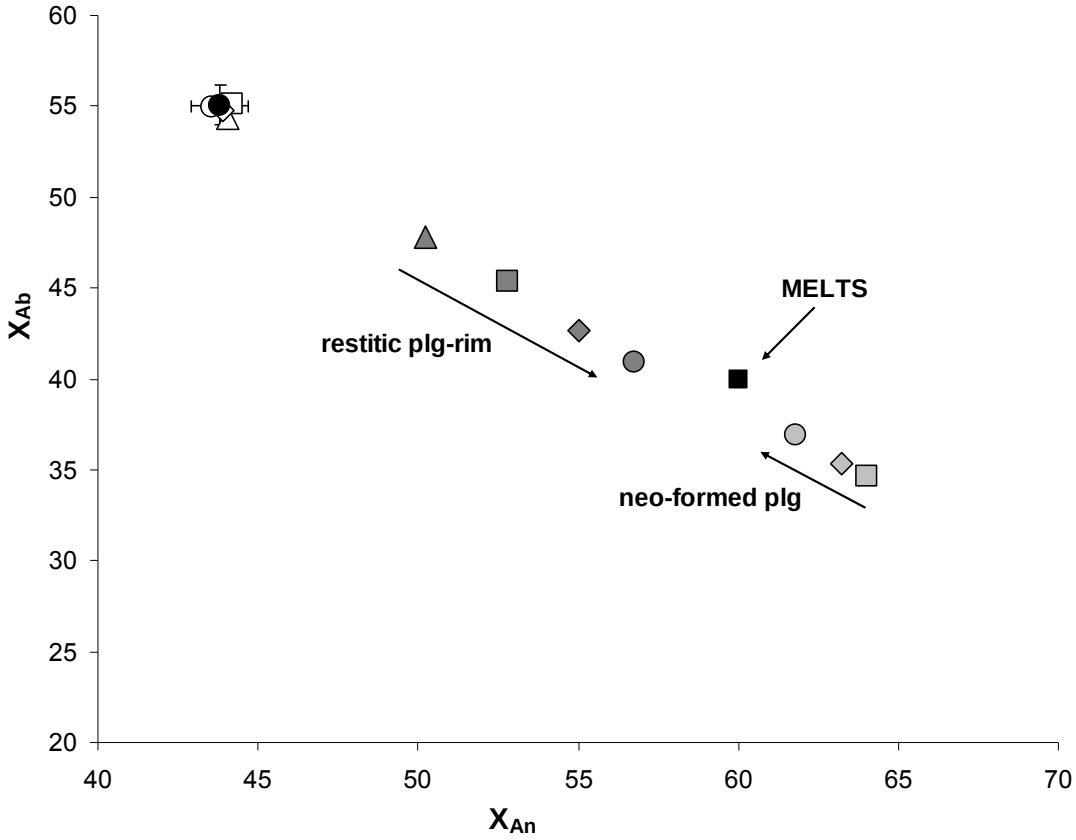


*Figure 3.2.1. Variability of plagioclase compositions. Closed circle: natural plg composition. Open symbols: MK72 restitic plg-core analyses. Dark grey symbols: MK72 restitic plg-rim analyses. Clear grey symbols: new-plg compositions. Triangles: 1 h time. Squares: 2 h time. Diamonds: 4 h time. Circles: 8 h time. $X_{An}$=anorthite molar fraction. $X_{Ab}$=albite molar fraction.*

New-plg show with time a chemical variability more restricted and in the opposite direction (i.e. increasing Ab content) compared with the one displayed by the rims of residual crystals (fig.3.2.1) .

Fig. 3.2.1 evidences a proceeding mixing between crustal and basaltic melts which is not linked to a diffusive process, as suggested by the melt compositions (later reported) around the interaction zone.

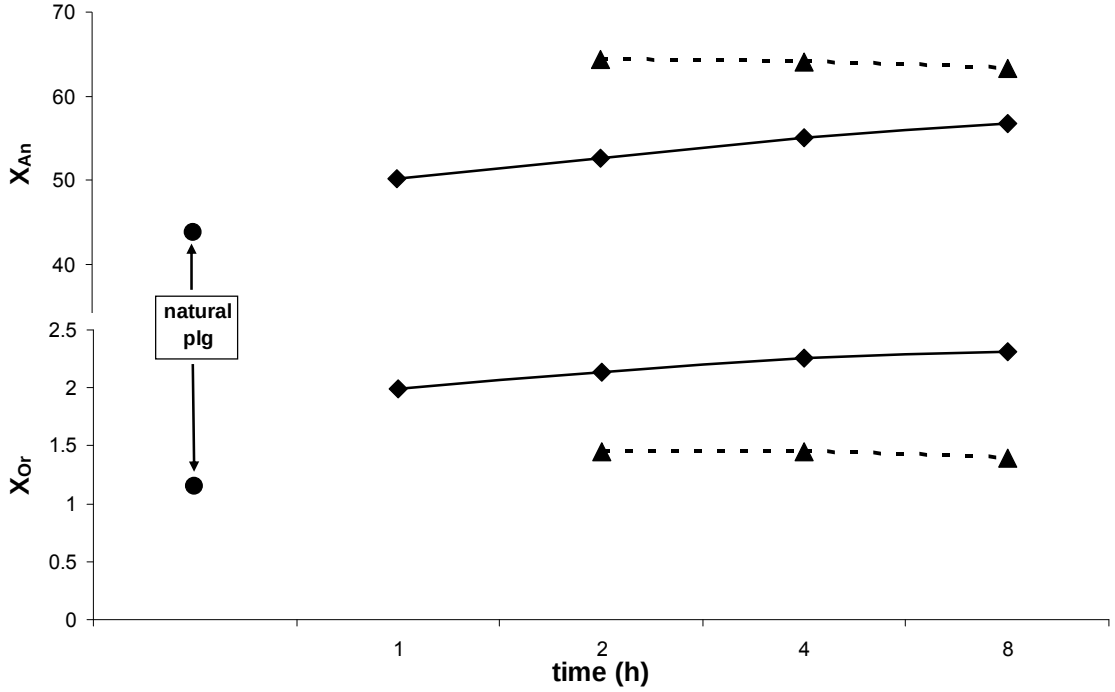


*Figure 3.2.2. Variability of plagioclase compositions. Closed circle: natural plg composition. Closed diamonds: MK72 restitic plg-rim analyses. Closed triangles: new-plg compositions. $X_{An}$=anorthite molar fraction. $X_{Or}$=orthoclase molar fraction.*

*3.3 Glass chemistries*

At the established P-T experimental conditions, crystallization did not occur in the PF1 melt, where the $H_2O$ amount was estimated to be 1 wt% by FTIR measurements, comparable with the original amount in the natural composition. PF1 glass chemistries are constant and similar to the PF1 starting one (table 3.3.1). Iron loss towards the walls of the Pt capsule was not observed, probably as a consequence of the short run duration and of the fairly high $fO_2$.

*Table 3.3.1. PF1 glass chemistries. Analyses are the average of 10 microprobe analyses.*

| wt% | 1 h | σ | 2h | σ | 4 h | σ | 8 h | σ |
|---|---|---|---|---|---|---|---|---|
| $SiO_2$ | 52.32 | 0.52 | 52.27 | 0.53 | 52.25 | 0.50 | 52.23 | 0.52 |
| $TiO_2$ | 0.59 | 0.01 | 0.61 | 0.01 | 0.59 | 0.03 | 0.53 | 0.02 |
| $Al_2O_3$ | 16.65 | 0.17 | 16.66 | 0.15 | 16.82 | 0.18 | 16.72 | 0.16 |
| FeO | 9.44 | 0.08 | 9.34 | 0.10 | 9.42 | 0.05 | 9.42 | 0.09 |
| MnO | 0.15 | - | 0.18 | - | 0.16 | - | 0.17 | - |
| MgO | 7.06 | 0.07 | 7.15 | 0.09 | 7.09 | 0.06 | 7.14 | 0.07 |
| CaO | 11.00 | 0.10 | 11.00 | 0.08 | 10.91 | 0.12 | 10.98 | 0.11 |
| $Na_2O$ | 1.79 | 0.02 | 1.80 | 0.02 | 1.80 | 0.03 | 1.81 | 0.01 |
| $K_2O$ | 0.84 | 0.01 | 0.87 | 0.02 | 0.86 | 0.04 | 0.86 | 0.01 |
| $P_2O_5$ | 0.15 | - | 0.12 | - | 0.11 | - | 0.13 | - |
| Total | 100.00 | | 100.00 | | 100.00 | | 100.00 | |
| Total* | 99.01 | | 99.05 | | 99.09 | | 99.10 | |

*original microprobe total

The MK72 melts change in composition accounting for the progressive plagioclase melting with time (table 3.3.2), as suggested by the increasing amounts of $Al_2O_3$ and $Na_2O$ and by mass balance calculations. The numerical approach results in a plagioclase contribution to the melt, from 20 to 35 wt% with time and is confirmed, within the analytical error, by FE-SEM analysis.

*Table 3.3.2. MK72 glass compositions. Values are the average of 10 microprobe analyses.*

| Run# | PC177 | | PC219 | | PC218 | | PC254 | |
|---|---|---|---|---|---|---|---|---|
| time (h) | 1 | | 2 | | 4 | | 8 | |
| wt% | | σ | | σ | | σ | | σ |
| $SiO_2$ | 47.24 | 1.17 | 48.10 | 0.96 | 48.83 | 0.53 | 49.46 | 0.49 |
| $TiO_2$ | 2.09 | 0.05 | 1.91 | 0.04 | 1.77 | 0.04 | 1.64 | 0.02 |
| $Al_2O_3$ | 23.77 | 0.59 | 24.03 | 0.48 | 24.25 | 0.28 | 24.44 | 0.24 |
| FeO | 6.36 | 0.18 | 5.82 | 0.13 | 5.38 | 0.10 | 4.99 | 0.06 |
| MnO | 0.14 | - | 0.13 | - | 0.12 | - | 0.11 | - |
| MgO | 2.77 | 0.07 | 2.54 | 0.05 | 2.34 | 0.03 | 2.17 | 0.02 |
| CaO | 10.85 | 0.27 | 10.68 | 0.21 | 10.53 | 0.14 | 10.41 | 0.10 |
| $Na_2O$ | 5.05 | 0.13 | 5.17 | 0.10 | 5.27 | 0.05 | 5.40 | 0.05 |
| $K_2O$ | 0.76 | 0.02 | 0.71 | 0.01 | 0.67 | 0.02 | 0.60 | 0.01 |
| $P_2O_5$ | 0.98 | 0.02 | 0.90 | 0.02 | 0.82 | 0.01 | 0.77 | 0.01 |
| Total | 100.00 | | 100.00 | | 100.00 | | 100.00 | |
| Total* | 99.25 | | 99.28 | | 99.30 | | 99.32 | |

*original microprobe total

Within the interaction layer developed at the contact of the two different rocks, a compositional gradient does exist but it changes with time thus preventing any estimate of diffusion coefficient/s. This is clearly evidenced in fig. 3.3.1 where the chemical variations measured along profiles perpendicular to the PF1/MK72 interface, at different times are graphically reported. Two distinct strips are evidenced. The first (clear grey), starting from the PF1 composition, represents the glassy portion of the PF1/MK72 interaction zone, where the chemical variations have been continuously detected; the second strip (dark grey), adjoining to the first, represents the layer where new formed crystals of plagioclase nucleated. Here, the interference of crystals just below the polished surface prevented reliable glass chemistries to be obtained and we preferred to not report the analyzed data. The analytical profiles show a substantial chemical modification in the MK72 domain, due to the increasing degree of melting in the meta-anorthosite; as a consequence, chemical variations measured along the profiles are produced by the starting chemical gradients of the elements. A further complication rises from the plagioclase crystallization. In fact, chemical variations are not consistent with a pure mixing between the MK72 and PF1 liquids as it should be (Yoder, 1973). The influence of the crystallizing mineral is well evidenced comparing data in tables 3.3.3 and 3.3.2. In table 3.3.3 the average

compositions corresponding to the middle of the chemical variations measured along the profiles are reported. Decreasing amounts of $Al_2O_3$ and $Na_2O$ and relative increases the other elements are not consistent with the opposite behaviour in MK72 melts, for a constant PF1 composition. The opposite features can be reconciled only when subtraction of a rough amount of 10 wt% of plagioclase is operated.

*Table 3.3.3. Melt compositions in the clear grey layer as function of time duration. Values are the average of 20 different microprobe analyses close to the dark-grey interaction layer.*

| Run# | PC177 | | PC219 | | PC218 | | PC254 | |
|---|---|---|---|---|---|---|---|---|
| time (h) | 1 | | 2 | | 4 | | 8 | |
| wt% | | σ | | σ | | σ | | σ |
| $SiO_2$ | 51.80 | 1.04 | 51.89 | 1.00 | 51.92 | 1.09 | 52.06 | 0.98 |
| $TiO_2$ | 0.80 | 0.02 | 0.81 | 0.04 | 0.83 | 0.02 | 0.85 | 0.01 |
| $Al_2O_3$ | 17.61 | 0.35 | 17.28 | 0.24 | 16.95 | 0.36 | 16.69 | 0.17 |
| FeO | 8.71 | 0.17 | 8.89 | 0.14 | 9.13 | 0.19 | 9.28 | 0.11 |
| MnO | 0.18 | 0.03 | 0.18 | 0.01 | 0.19 | 0.04 | 0.20 | 0.01 |
| MgO | 6.00 | 0.12 | 6.27 | 0.10 | 6.59 | 0.14 | 6.77 | 0.07 |
| CaO | 10.89 | 0.21 | 10.83 | 0.15 | 10.75 | 0.23 | 10.63 | 0.11 |
| $Na_2O$ | 2.99 | 0.06 | 2.83 | 0.03 | 2.61 | 0.05 | 2.49 | 0.03 |
| $K_2O$ | 0.83 | 0.02 | 0.84 | 0.01 | 0.85 | 0.02 | 0.86 | 0.01 |
| $P_2O_5$ | 0.19 | - | 0.18 | - | 0.18 | - | 0.17 | - |
| Total | 100.00 | | 100.00 | | 100.00 | | 100.00 | |
| Total* | 99.12 | | 99.15 | | 99.16 | | 99.18 | |

*original microprobe total

Because within the interaction zone the plagioclase composition is practically constant with time, it is reasonable to infer that the melt from which crystals nucleate, operates as a “buffer layer” between the PF1 and the MK72 compositions. It means that here, melt composition is kept constant through a selective elements migration from the adjoining melts, thus modifying the effective diffusion rates otherwise obtainable in absence of crystal nucleation and growth.

Melt compositions are still basaltic andesite even with a slight D.I. increment with respect to the basaltic starting material.

Fig. 3.3.2a-b show the variations of differentiation index (D.I.) and Mg-number (Mg#) of the hybrid melts compared to those of the PF1 glass. As the experimental time increases, the hybridized compositions become less differentiated and the Mg# of the 8 h experimental run, results more similar to that of the PF1 original composition. The long time-run composition is still $Na_2O$-rich and Mg#-poor compared to the PF1 chemistry.

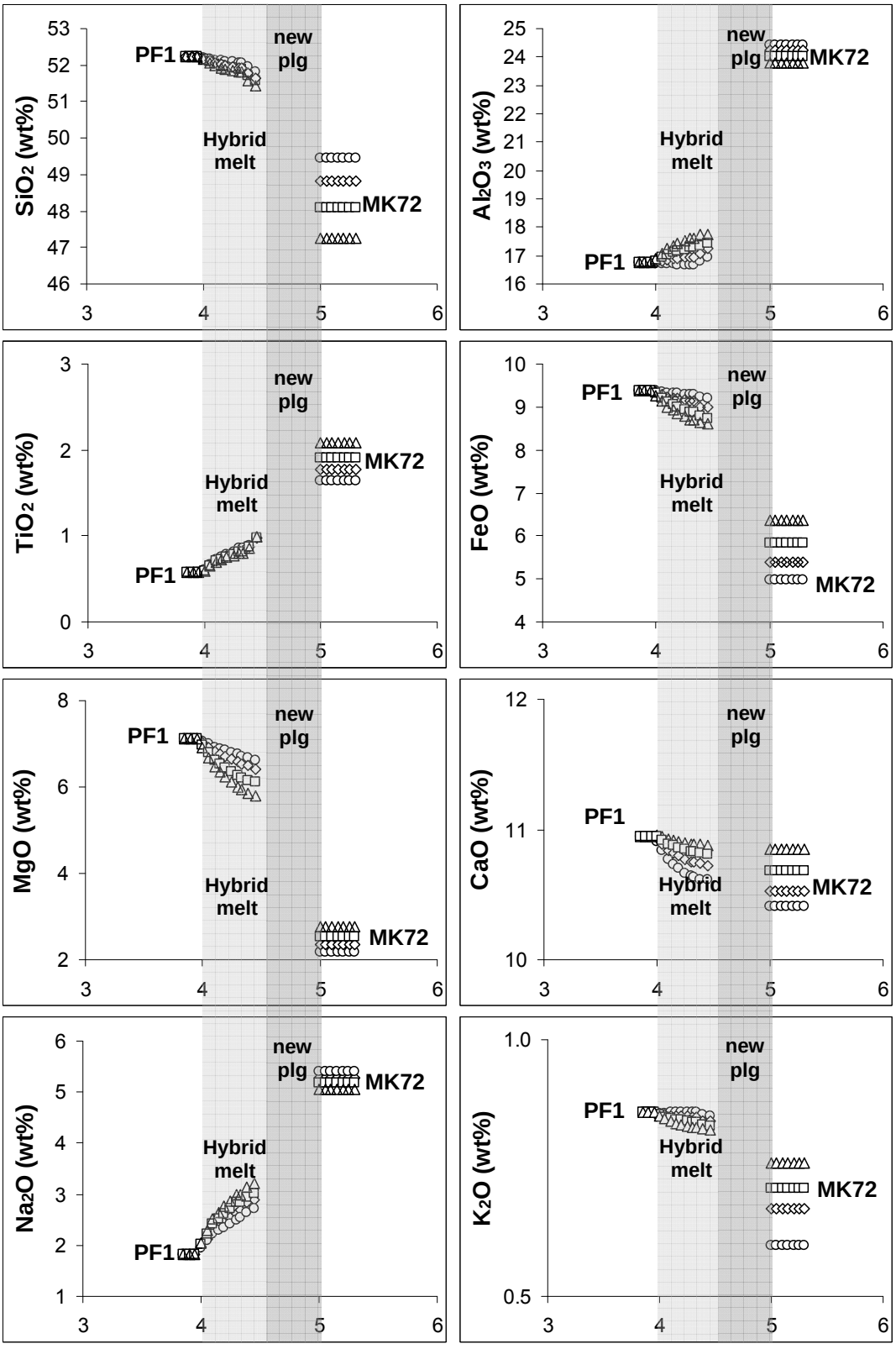


*Figure 3.3.1. Compositional profiles of the basalt-granulite reaction boundary layers. Profiles are measured along the length axis of the capsules. Open triangles: 1 h time. Open squares: 2 h time. Open diamonds: 4 h time. Open circles: 8 h time.*

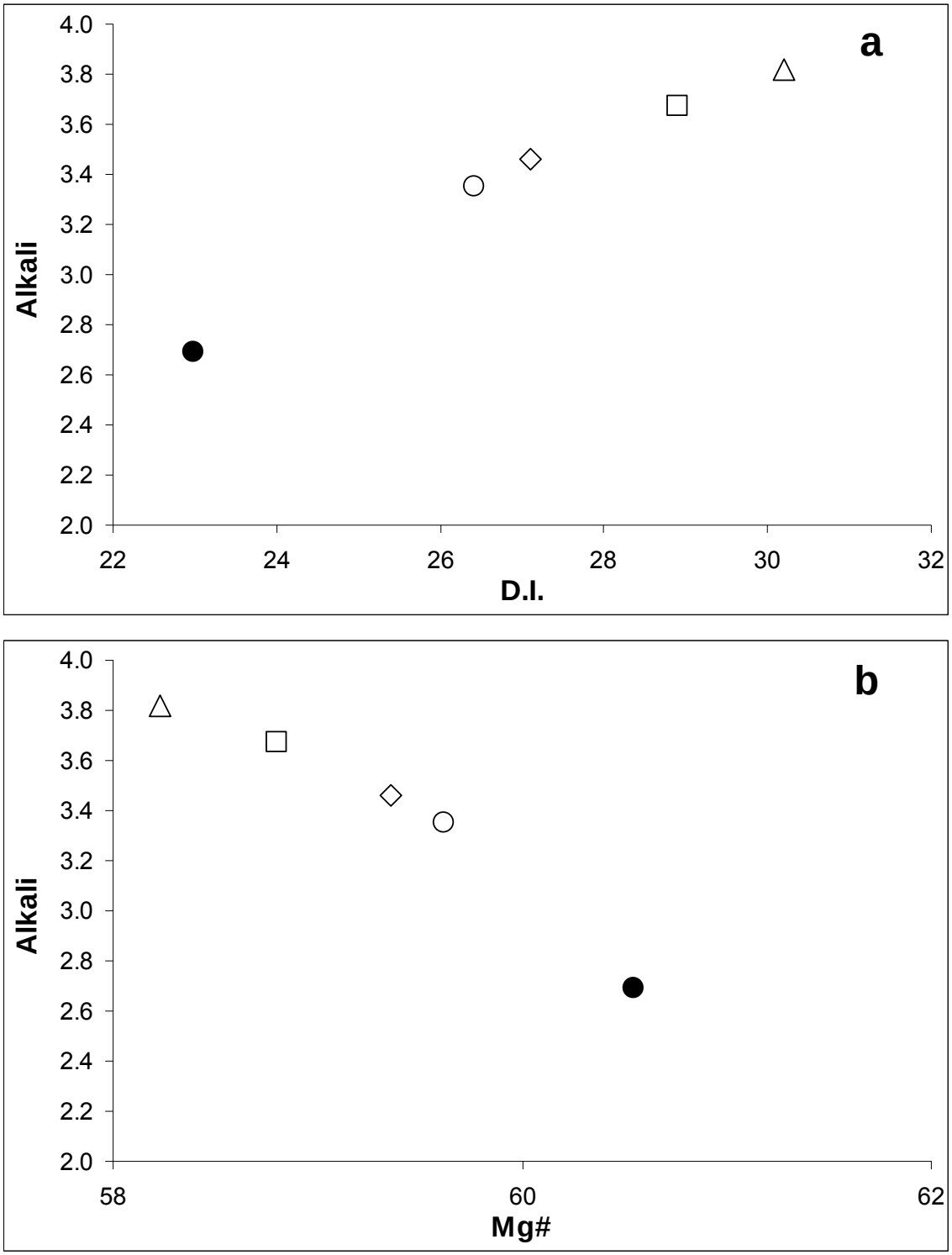


*Figure 3.3.2. Melt modifications in the clear grey layer as function of time duration compared to PF1. Closed circle: bulk compositions of basalt. Open triangles: 1 h time. Open squares: 2 h time. Open diamonds: 4 h time. Open circles: 8 h time.*

*3.4 Trace element variations*

Trace elements distribution between PF1 and MK72 was measured only in the 8 h experimental run, because, as discussed above, produced compositions are approaching those corresponding to stationary conditions. To obtain a good statistic number of analyses, three parallel profiles were analyzed across the PF1/MK72 contact (fig. 3.4.1). Processing the obtained data was complex because of the impossibility to discriminate from glass, neo-plagioclases, and restitic plagioclases smaller than the laser beam (25 μm). Such inconvenient caused the screening of all the data obtained after each analyzed profile; moreover, to better constrain the position of the points within the interaction layer, a fourth profile transversal to the interaction zone was analyzed (fig. 3.5.1).

.

Fig. 3.4.2 reports the analytical profiles of some selected trace elements. A clear "diffusion like" S-shaped profile is evidenced for most elements. Nevertheless their trends are not consistent with those usually reported in literature. A steep ramp, starting from PF1 towards MK72 side, led to some anomalous amounts, in the hybrid glass, higher than in both starting materials.

It must be noted that such behaviour, as well as the S-shaped trends are not observed for the elements that have a low or null concentration gradient between the two starting compositions (fig. 3.4.3). When present, these irregular trends are independent from the original gradients, atomic number, ionic radius, charge, and field strength of the chosen element. We think that plagioclase crystallization is at the origin of the anomalous enrichments even if the key relations are not clear; in fact, if it is possible suppose that in the interacting layer melt becomes enriched in elements not compatible with plagioclase, it is not obvious why the same happens, even at minor extent, to Sr. What is evident, however, is that in presence of crystals, diffusion of trace elements is no more driven by gradients between the previous compositions but the interacting melt acts as a new starting interacting material.

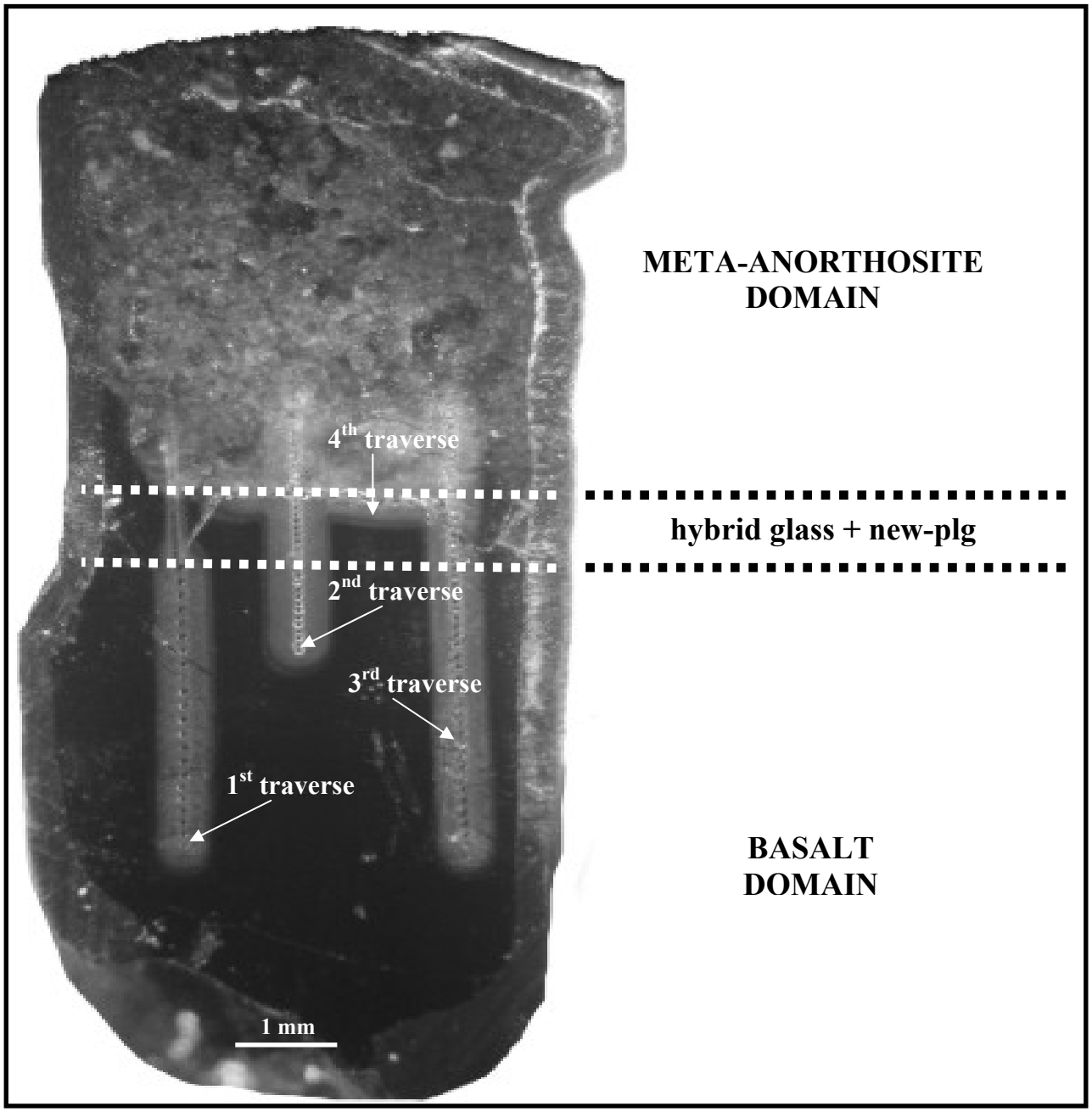


*Figure 3.4.1. LA-ICP-MS analytical spots performed on the 8 h experimental run.*

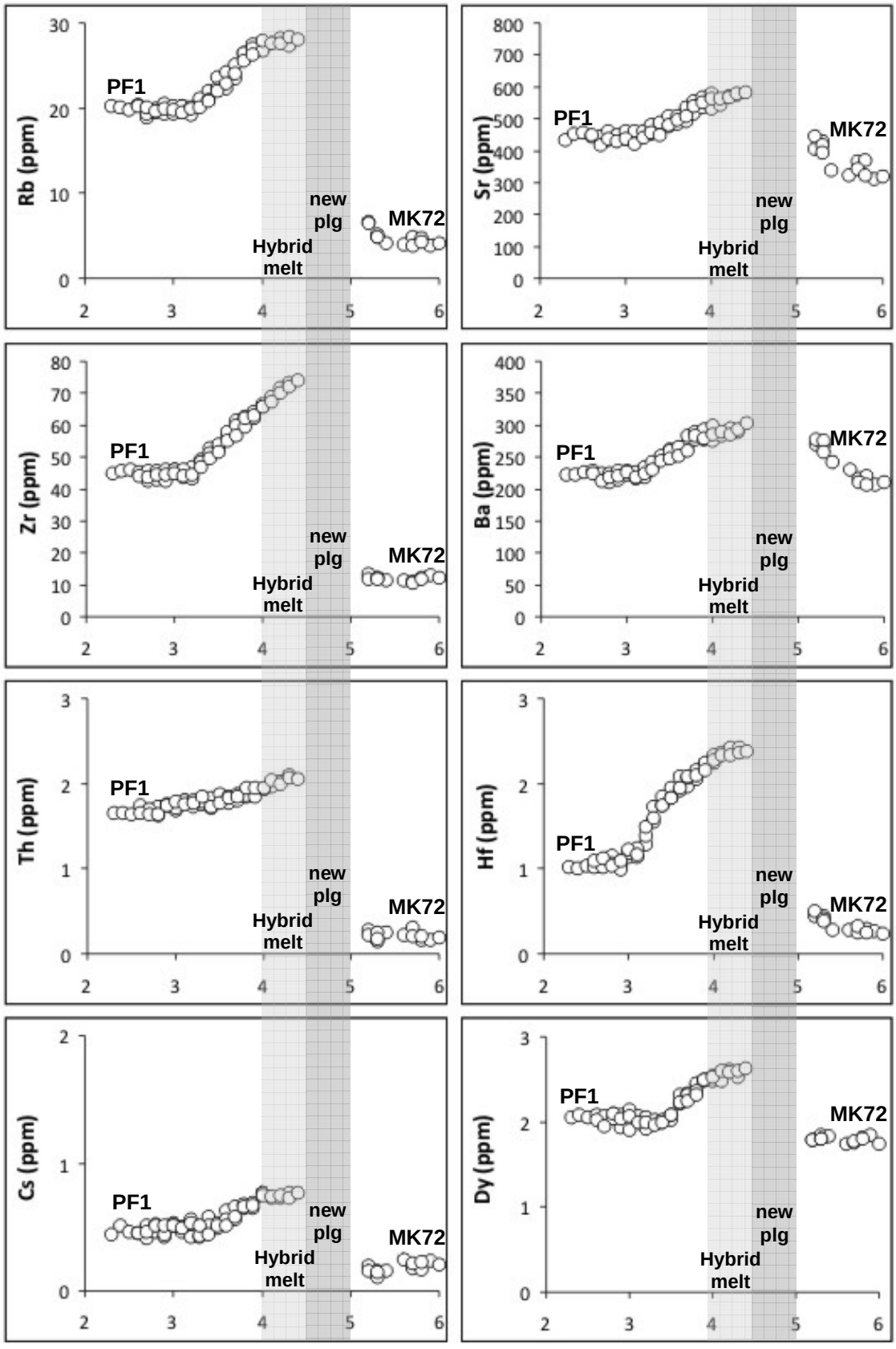


*Figure 3.4.2. Selected trace element chemical profiles that show anomalous enrichments in the hybrid melt.*

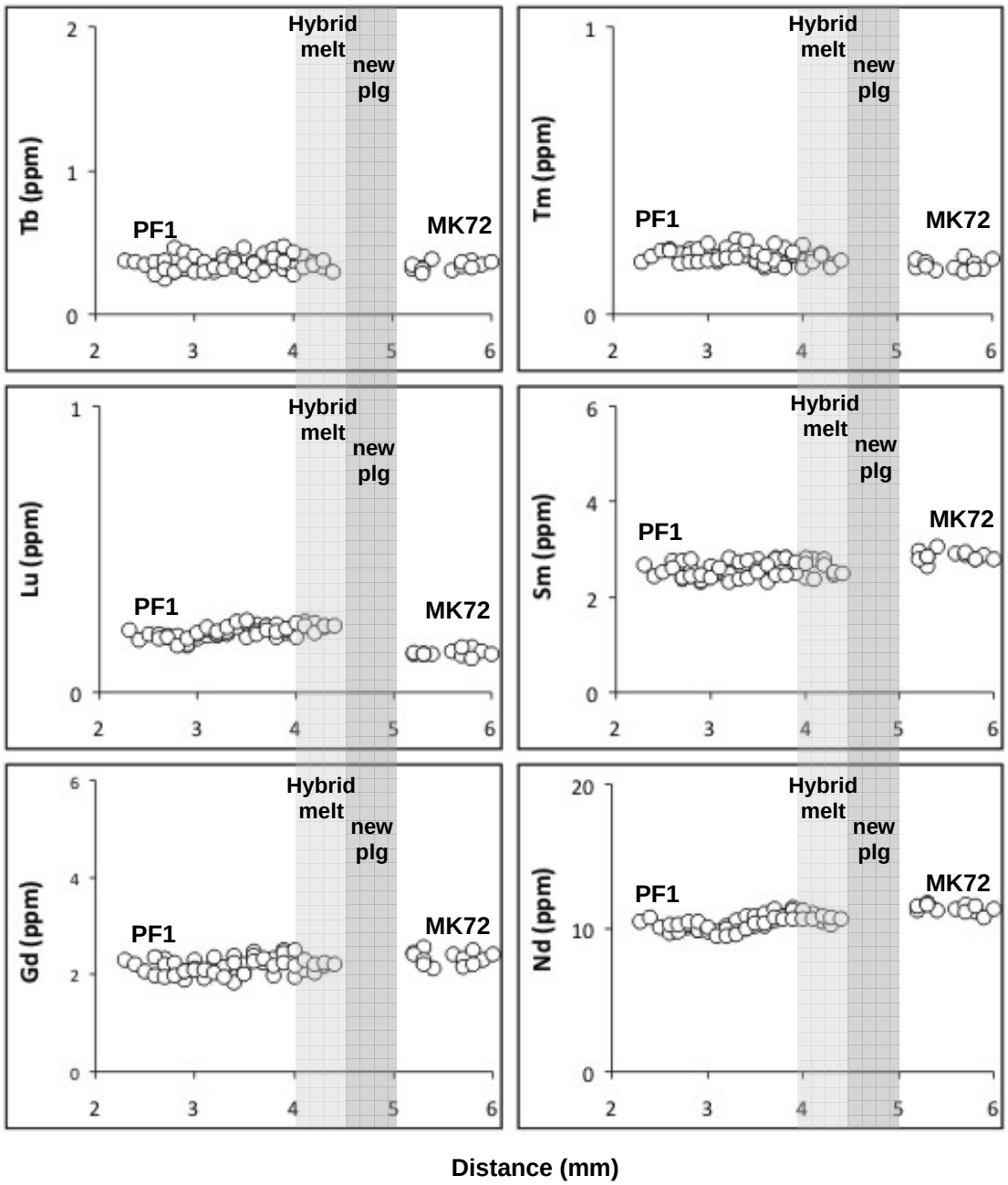


*Figure 3.4.3. Selected trace element chemical profiles that do not show chemical variations in the PF1 and MK72 glass composition.*

# 4 - Basalt/metapelite interaction

Run conditions and experimental configurations are illustrated in table 4.1.1.

Products obtained in the PF1/VA38 coupled experiments consist of a partially crystallized basalt below a partially molten metapelite.

A multisaturation at 1150 °C with two pyroxene and plagioclase has been confirmed by MELTS calculations for the PF1 basaltic composition, both under anhydrous and water-bearing conditions; calculated liquidus temperatures result in 1230 °C (anhydrous) and 1200 °C (1 wt% water). According to MELTS the estimated liquidus temperature for the metapelite composition should have been 1080°C, well below the experimental one. The restitic assemblage found in our experiments is thus related to kinetics.

*Table 4.1 Experimental runs and conditions.*

| Run# | T (°C) | P (Gpa) | t (h) | $H_2O$* (wt%) | starting material | products |
|---|---|---|---|---|---|---|
| PC256 | 1150 | 0.5 | 1 | 0.8 | PF1/VA38 | 2px+plg+g/q+sil+g |
| PC258 | 1150 | 0.5 | 2 | 1.0 | PF1/VA38 | 2px+plg+g/q+sil+g |
| PC257 | 1150 | 0.5 | 4 | 0.9 | PF1/VA38 | 2px+plg+g/q+sil+g |
| PC287 | 1150 | 0.5 | 8 | 1.1 | PF1/VA38 | 2px+plg+g/q+sil+g |
| PC256 | 1150 | 0.5 | 1 | - | VA38 | q+sil+g |
| PC258 | 1150 | 0.5 | 2 | - | VA38 | q+sil+g |
| PC257 | 1150 | 0.5 | 4 | - | VA38 | q+sil+g |
| PC287 | 1150 | 0.5 | 8 | - | VA38 | q+sil+g |

*amount of added water to the basaltic composition

## *4.1 Textural characters*

Crystals of pyroxene and plagioclase nucleate in the basaltic liquid (fig. 4.1.1), settling through the molten fraction toward the lower portion of the capsule. Crystal settling becomes evident with increasing run duration so that, at the end of the most prolonged run the lower part of the capsule appears enriched in crystals, while the upper portion is full glass (fig. 4.1.2).

Mineral dimensions, measured by FE-SEM image analyses in the 4 and 8 h products, range from 10 to 70 μm. Such variation, even if partially related to the

anisotropic shape of the crystals, is mainly function of the experimental time because larger sizes have been statistically found in the 8 h run. Percent of crystallization was difficult to estimate by SEM image, because of crystals sinking. Results from FE-SEM chemical maps, mediated for the entire length of the basaltic domain, and mass balances, give a percentage increasing with time (~4→18 vol%) and a pyroxene/plagioclase almost constant ratio (~1.5 ). It must to be pointed that the crystallization rate is not constant, being higher within 4 hours and decreasing substantially after this span of time, so that melt composition in the 8 h run can be considered close to the equilibrium values.

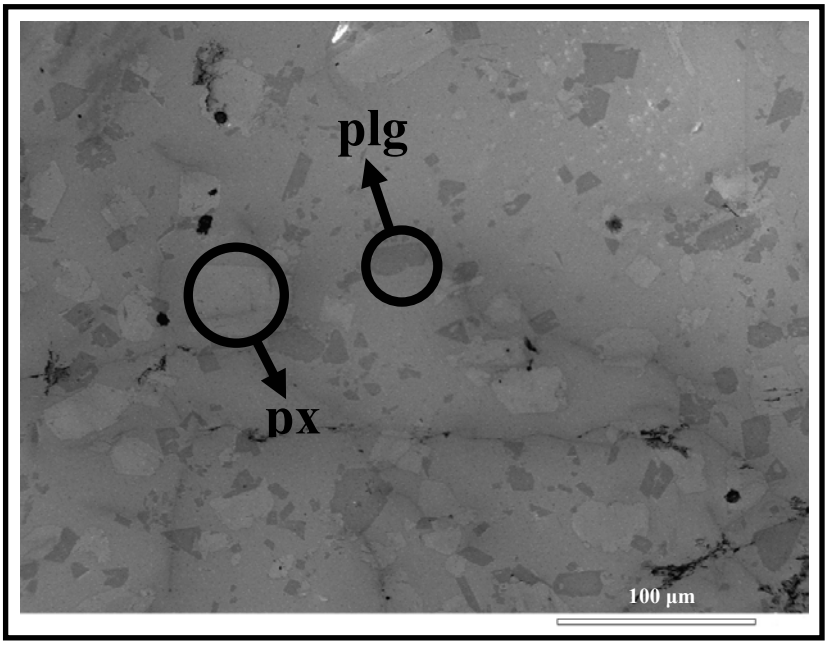


*Figure 4.1.1. FE-SEM BSE image of PF1 8h run.*

A rough estimate of the sinking velocity of the crystals was performed applying the Stoke law. Melt density (2.68 g/cm$^3$) and viscosity (1250 poise) have been calculated starting from the glass chemistries and the amount of added water, using the relations and the P-T variations of the adopted parameters as reported by Lange & Carmichael (1987) and Giordano et al. (2006), respectively. The total iron amount was partitioned between $Fe_2O_3$ and FeO at the estimated NNO+2 oxygen fugacity, according to Kress & Carmichael (1988). To estimate the crystal sinking velocities we consider them spherical with an average diameter of 60 µm.

The chosen pyroxene density was 3.3 g/cm$^3$, while for plagioclase a density of 2.72 g/cm$^3$ was calculated accounting for the amount of albite and anorthite components (table 4.2.1). Results give a travelled distance of ~3 mm and ~1.5 mm after 8 h for pyroxene and plagioclase respectively, assuming a newtonian behaviour of the liquid. Such picture is not in contrast with the analyzed distribution of the crystals in the 8 h run. Here crystals are distributed in a 2 mm thick layer where their estimated amount is averaging 20 vol%. Such amount turns the liquid toward a binghamian behaviour with a yield strength in the range $10^3$ dyne/cm$^2$ so that the minimum radius for the crystal to settle becomes higher than that measured in our crystals preventing ulterior sinking of the solids.

The contact between PF1 and VA38 in all the run-products is marked by a fracture line, dividing the dark, metapelitic domain from the clear basaltic glass (fig. 4.1.2). The thickness of the interaction layer, approximately 2 mm, keeps constant with time and is revealed only through the chemical variations in the glass. As discussed by previous authors (Johnston & Wyllie, 1988; Van Der Laan & Wyllie, 1993), it is unlikely this boundary matches the original PF1/VA38 contact. However we guess it fairly preserves the starting position for the following considerations: 1) during capsule filling the thickness of the two powders were measured and similar thickness has been found after each run; 2) FE-SEM image analyses did not reveal the presence of vapour bubbles in both VA38 and PF1 glasses thus excluding that convective processes played a significant role. These considerations rule out the possibility that basalt crystallization and the increasing amount of melt in VA38 upon heating up to 1150 °C, could have significantly modified the starting planar surface between the two compositions.

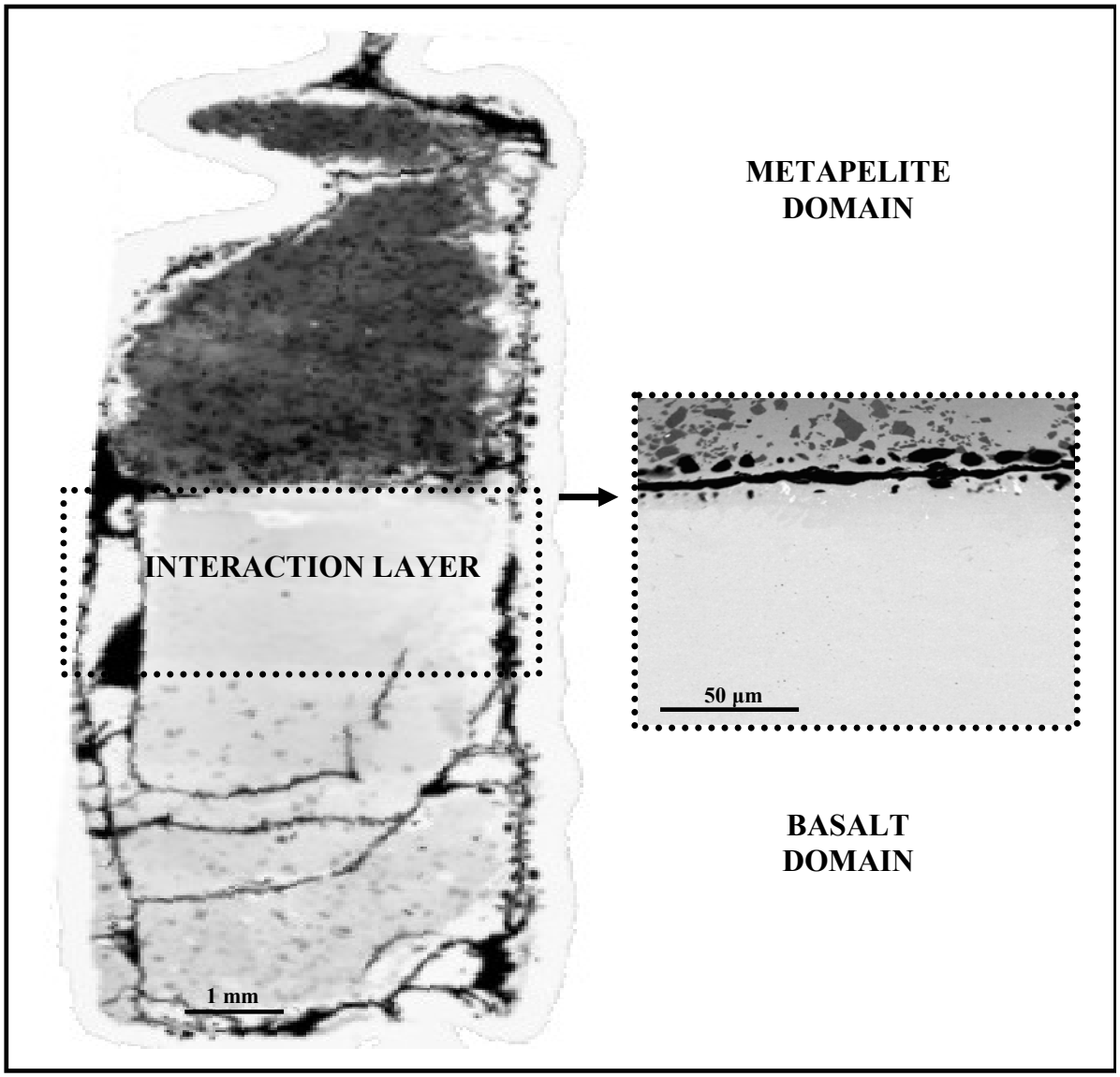


*Figure 4.1.2. FE-SEM image of the capsule assemblage after 4 h run.*

The metapelitic rock-powder is not completely melted. Restitic assemblage in VA38, consists of quartz grains plus small, elongated crystals of sillimanite, with resorbed edges. Crystals, in the shortest time runs, range in size within 30-50 µm, but their dimensions decrease with time down a maximum length of 20 µm. Minerals have been detected by FE-SEM BSE analyses (fig. 4.1.3). Textural characters are the same when coupled PF1/VA38 and simple VA38 products are compared.

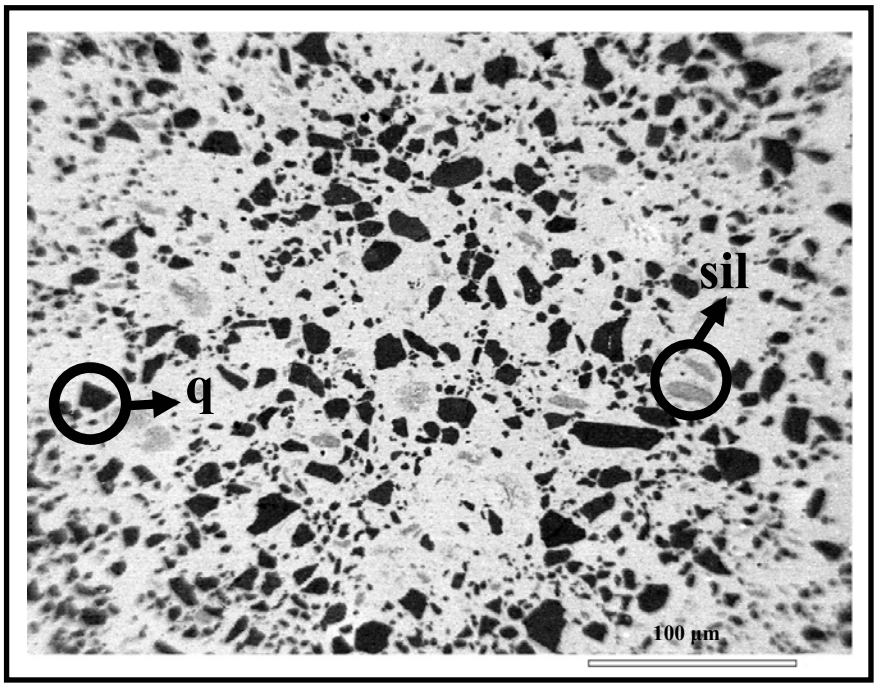


*Figure 4.1.3. Metapelite texture after 2 h run. FE-SEM BSE image.*

*4.2 Mineral chemistries*

As previously referred, basalt is partially crystallized. Bytwonite plagioclase plus ortho- and clino-pyroxenes have been analyzed. Microprobe analyses do not evidence crystal zoning and no chemical variations has been detected as function of time. Mineral chemistries are reported in table 4.2.1. and coexisting pyroxenes are plotted into the En-Fs-Di-Hd quadrilateral (fig. 4.2.1).

Orthopyroxene shows fairly high amounts of alumina and calcium, which are not fully consistent with the $Al_2O_3$ detected in the Ca-rich clinopyroxene, or with the CaO amount of the coexisting melt. A possible, slight glass contamination may have altered the results, accounting for the small size of the analyzed crystals. Occurrence of $Fe^{+3}$ can be ascribed to the relatively high oxygen fugacity during the experiments. Tie line between Ca-rich- and Ca-poor-pyroxene evidences a similar magnesium-iron partition .

*Table 4.2.1. Mineral analyses of the basalt assemblage. Reported values are the average of 10 microprobe spots.*

| Phase | opx | | cpx | | | plg | |
|---|---|---|---|---|---|---|---|
| wt% | | σ | | σ | | | σ |
| $SiO_2$ | 53.69 | 0.18 | 50.30 | 0.10 | $SiO_2$ | 47.02 | 0.29 |
| $TiO_2$ | 0.15 | 0.06 | 0.32 | 0.02 | $TiO_2$ | - | - |
| $Al_2O_3$ | 3.55 | 0.17 | 3.96 | 0.09 | $Al_2O_3$ | 33.13 | 0.25 |
| FeO | 10.74 | 0.14 | 6.42 | 0.07 | $Fe_2O_3$ | 1.03 | 0.02 |
| MnO | 0.31 | 0.02 | 0.14 | 0.02 | MnO | - | - |
| MgO | 28.58 | 0.13 | 16.12 | 0.11 | MgO | - | - |
| CaO | 2.99 | 0.17 | 22.56 | 0.05 | CaO | 16.93 | 0.29 |
| $Na_2O$ | - | - | 0.19 | - | $Na_2O$ | 1.85 | 0.08 |
| $K_2O$ | - | - | - | - | $K_2O$ | 0.04 | - |
| Total | 100.00 | | 100.00 | | Total | 100.00 | |
| Total* | 99.56 | | 99.63 | | Total* | 99.75 | |
| | | | | | | | |
| Si | 1.910 | | 1.852 | | Si | 2.165 | |
| Ti | 0.004 | | 0.009 | | Al | 1.798 | |
| $Al^{IV}$ | 0.090 | | 0.148 | | Fe | 0.036 | |
| $Al^{VI}$ | 0.037 | | 0.001 | | Ca | 0.835 | |
| $Fe^{3+}$ | 0.030 | | 0.095 | | Na | 0.165 | |
| $Fe^{2+}$ | 0.290 | | 0.102 | | K | 0.002 | |
| Mn | 0.009 | | 0.004 | | | | |
| Mg | 1.516 | | 0.885 | | | | |
| Ca | 0.114 | | 0.890 | | | | |
| Na | - | | 0.013 | | | | |

*original microprobe total

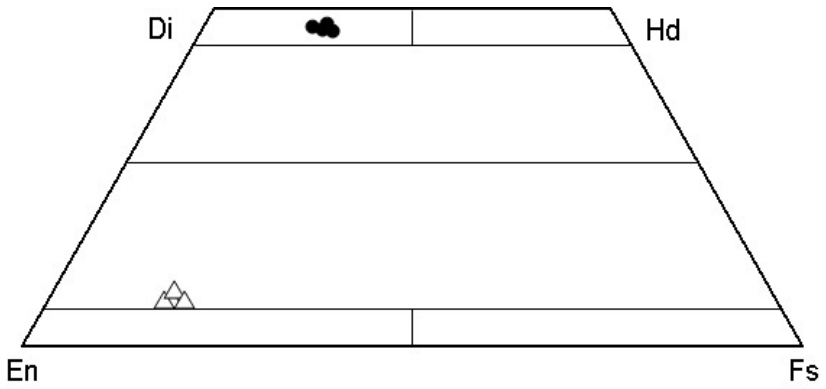


*Figure 4.2.2. Mineral chemistries plotted in the pyroxene quadrilateral.*

*4.3 Glass chemistries*

Crystallization moves the starting PF1 composition towards more differentiated melts (PF1*) whose compositions are reported in table 4.3.1; chemistries are still basaltic, slightly shifted to the basaltic andesite boundary.

*Table 4.3.1. PF1* differentiated melt compositions. Values are the average of 10 microprobe analyses.*

| RUN# | PC256 | | PC258 | | PC257 | | PC287 | |
|---|---|---|---|---|---|---|---|---|
| time (h) | 1 | | 2 | | 4 | | 8 | |
| wt% | | σ | | σ | | σ | | σ |
| $SiO_2$ | 52.30 | 0.32 | 52.38 | 0.44 | 52.69 | 0.35 | 52.79 | 0.38 |
| $TiO_2$ | 0.60 | 0.04 | 0.60 | 0.03 | 0.63 | 0.04 | 0.62 | 0.03 |
| $Al_2O_3$ | 16.70 | 0.24 | 16.69 | 0.31 | 16.70 | 0.22 | 16.68 | 0.24 |
| FeO | 9.58 | 0.15 | 9.80 | 0.12 | 10.23 | 0.09 | 10.28 | 0.11 |
| MnO | 0.19 | 0.03 | 0.20 | 0.03 | 0.19 | 0.03 | 0.19 | 0.04 |
| MgO | 7.02 | 0.10 | 6.85 | 0.12 | 6.12 | 0.08 | 6.09 | 0.11 |
| CaO | 10.68 | 0.16 | 10.48 | 0.18 | 10.28 | 0.12 | 10.14 | 0.07 |
| $Na_2O$ | 1.91 | 0.08 | 1.87 | 0.10 | 1.96 | 0.09 | 1.98 | 0.08 |
| $K_2O$ | 0.88 | 0.05 | 0.99 | 0.05 | 1.05 | 0.07 | 1.07 | 0.05 |
| $P_2O_5$ | 0.14 | 0.03 | 0.14 | 0.02 | 0.15 | 0.03 | 0.16 | 0.03 |
| Total | 100.00 | | 100.00 | | 100.00 | | 100.00 | |
| Total* | 99.04 | | 98.81 | | 98.78 | | 98.53 | |

*original microprobe total

Data reported in the above table, are averaged from the lower portion of the basaltic domain, because the upper glassy layer, although preserving most of major elements ratios, evidences clear signs of alkali diffusion, as illustrated by fig. 4.3.1. Chemical profiles perpendicular to the basalt-metapelite interface, are reported for $K_2O$ and $Na_2O$, i.e. the elements diffusing beyond the interaction layer (clear grey strip in fig. 4.3.1).

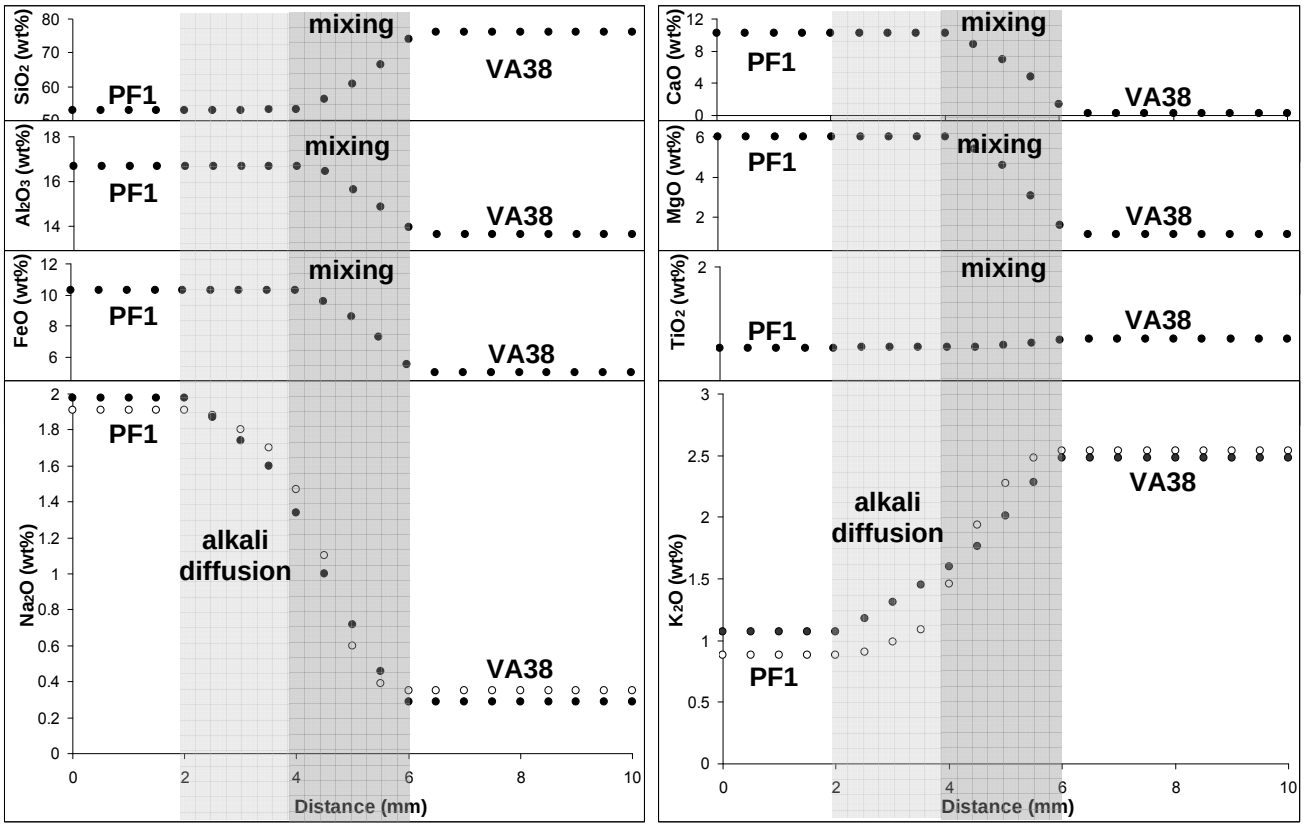


*Figure 4.3.1. Chemical profiles after 1 and 8h run. Open circles: 1 h time. Closed circle: 8 h time.*

Element concentrations in the PF1/VA38 interaction layer, vary continuously through a chemical gradient, according to an almost perfect mixing rule (dark grey strip in fig. 4.3.1). As example, five representative glass chemistries within the interaction domain, are reported in table 4.3.2. Analyses have been collected with a constant interval in the 8 h run , from the basalt boundary. Element variations evidence the spatial development of the mixing process.

*Table 4.3.2. Glass chemical variations in the interaction layer after 8 h run.*

| wt% | 4.3 | 4.6 | 4.9 | 5.2 | 5.5 |
|---|---|---|---|---|---|
| | (distance in mm) | | | | |
| $SiO_2$ | 53.46 | 56.35 | 60.81 | 66.52 | 73.93 |
| $TiO_2$ | 0.70 | 0.70 | 0.71 | 0.75 | 0.80 |
| $Al_2O_3$ | 16.56 | 16.44 | 15.63 | 14.87 | 13.96 |
| FeO | 10.19 | 9.58 | 8.62 | 7.29 | 5.49 |
| MnO | 0.19 | 0.18 | 0.17 | 0.15 | 0.13 |
| MgO | 6.16 | 5.37 | 4.60 | 3.08 | 1.63 |
| CaO | 10.10 | 8.90 | 7.01 | 4.80 | 1.33 |
| $Na_2O$ | 0.98 | 0.69 | 0.49 | 0.38 | 0.28 |
| $K_2O$ | 1.51 | 1.63 | 1.80 | 2.00 | 2.30 |
| $P_2O_5$ | 0.15 | 0.15 | 0.15 | 0.15 | 0.15 |
| Total | 100.00 | 100.00 | 100.00 | 100.00 | 100.00 |
| Total* | 98.73 | 98.68 | 98.65 | 98.55 | 98.25 |

*original microprobe total

VA38 glasses were analyzed either in PF1/VA38 coupled experiments, and in the VA38 run alone. Chemistries reveal a good homogeneity in both experiments (table 4.2.3). The obtained rhyolitic compositions display a slight variation in the $SiO_2/Al_2O_3$ ratio (5.26-5.58), increasing with run duration, thus suggesting a higher stability of the restitic sillimanite with respect to quartz. Nevertheless it must be considered that such variation could be addressed to the analytical uncertainties.

Previous authors observed in basalt-granite interaction experiments, an extensive alkali diffusion in the basaltic reservoir (Watson & Jurewictz, 1984; Watson & Baker, 1991; Koyaguchi, 1989). As authors reported in their works, the non-alkali slow-moving nature, provides a useful “reference frame” by which to gauge changes in the concentrations of Na and K. Present experiments give us the opportunity to estimate alkali diffusion coefficients in the studied system; a more extensive discussion will be reported in the next chapter.

*Table 4.3.3. Representative analyses of the partially molten metapelite melts at the experimental conditions. Values are the average of 10 microprobe analyses.*

| RUN# | PC256 | | PC258 | | PC257 | | PC287 | |
|---|---|---|---|---|---|---|---|---|
| time (h) | 1 | | 2 | | 4 | | 8 | |
| wt.% | | σ | | σ | | σ | | σ |
| $SiO_2$ | 75.86 | 0.44 | 75.98 | 0.48 | 76.02 | 0.38 | 76.14 | 0.35 |
| $TiO_2$ | 0.75 | 0.08 | 0.77 | 0.06 | 0.79 | 0.08 | 0.81 | 0.06 |
| $Al_2O_3$ | 14.20 | 0.28 | 14.00 | 0.22 | 13.84 | 0.24 | 13.65 | 0.28 |
| FeO | 4.88 | 0.22 | 4.91 | 0.24 | 4.94 | 0.18 | 4.96 | 0.22 |
| MnO | 0.11 | 0.07 | 0.11 | 0.07 | 0.13 | 0.07 | 0.13 | 0.08 |
| MgO | 1.00 | 0.20 | 1.05 | 0.18 | 1.11 | 0.16 | 1.14 | 0.22 |
| CaO | 0.18 | 0.18 | 0.21 | 0.16 | 0.24 | 0.18 | 0.25 | 0.14 |
| $Na_2O$ | 0.35 | 0.16 | 0.32 | 0.14 | 0.30 | 0.12 | 0.29 | 0.16 |
| $K_2O$ | 2.54 | 0.09 | 2.52 | 0.10 | 2.48 | 0.09 | 2.48 | 0.10 |
| $P_2O_5$ | 0.13 | 0.05 | 0.13 | 0.04 | 0.15 | 0.05 | 0.15 | 0.05 |
| Total | 100.00 | | 100.00 | | 100.00 | | 100.00 | |
| Total* | 98.07 | | 98.15 | | 98.10 | | 98.17 | |
| | | | | | | | | |
| $SiO_2/Al_2O_3$ | 5.34 | | 5.43 | | 5.49 | | 5.58 | |

*original microprobe total

*4.4 Trace element variations*

Trace elements distribution between basalt and metapelite melt was measured in the 8 h experimental run. Two parallel profiles were performed across the PF1/VA38 interaction layer (fig. 4.4.1), to obtain a good statistic number of analyses. Dataset interpretation revealed a slight disalignment of the points, for this reason they were shifted before comparing the overlapped data.

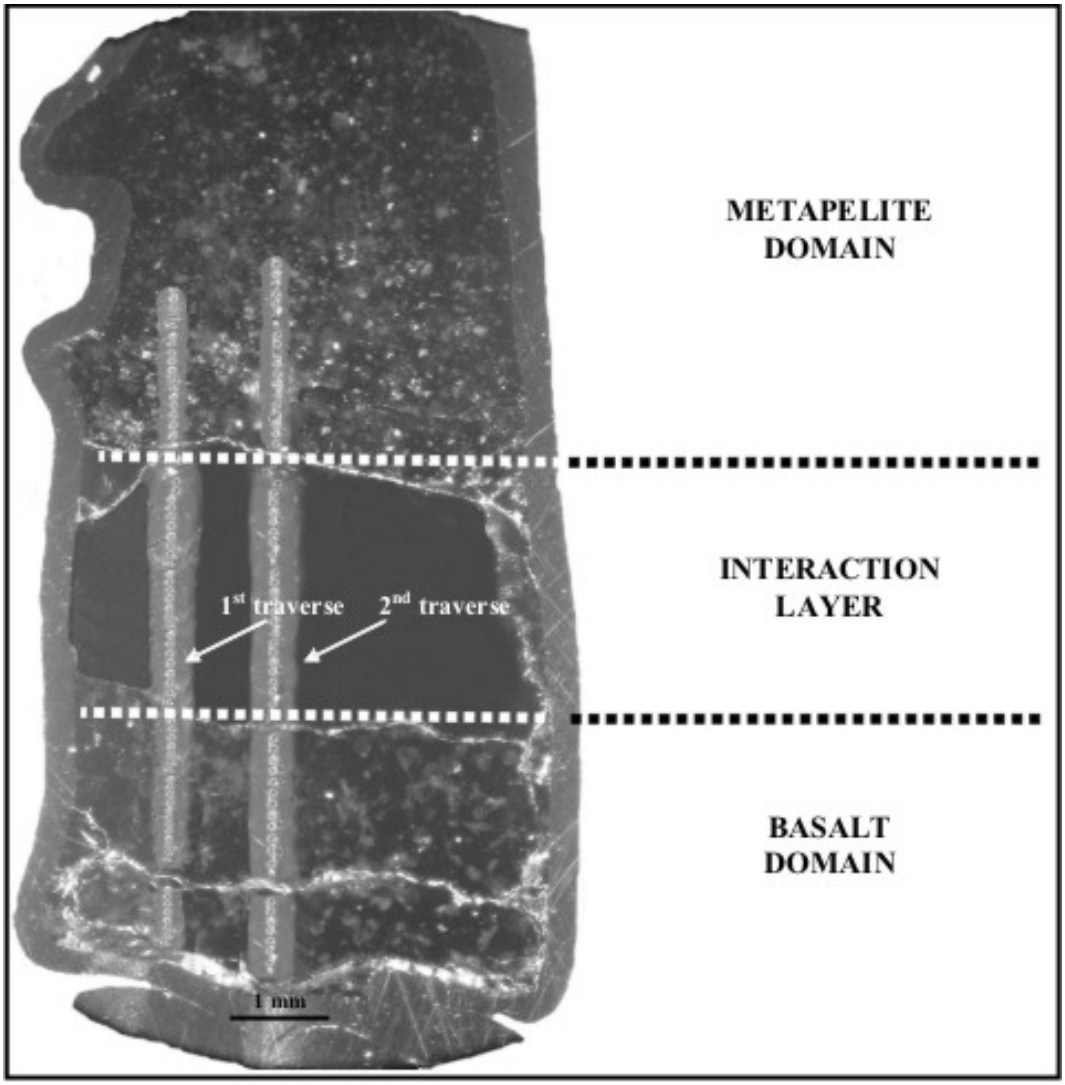


*Figure 4.4.1. LA-ICP-MS analytical spots performed on the 8 h experimental run.*

Chemical profiles of some representative elements are showed in fig. 4.4.2. Two constant chemical plateaux are observed, far from the interaction layer while mixing, S-shaped trends are present within it (dark grey strip in fig. 4.4.2). However, this behaviour is not observed for all the analyzed elements. Figure 4.4.3 shows as amounts of some others do vary from the basaltic reservoir to the interaction layer, according to a chemical flux opposite to their concentration gradients (clear grey strip).

These two different behaviours are not dependent on the geochemical grouping (LILE, REE, HFSE) of the analyzed elements; Rb, Sr, and Ba follow the same mixing rule of Nb, Ta, and Cs, whereas diffusive processes occur for the REE, and for Hf (HFSE) and Pb (heavy metals).

Trace element diffusion has been investigated by some authors in experimental studies performed at different P-T-X conditions (Hoffman, 1980; Jambon, 1982; Baker & Watson, 1988; Mungall & Dingwell, 1997; Nakamura & Kushiro, 1998). Results suggest that their abundance in igneous rocks, may be affected by diffusional processes at the magmatic stage. However, models in natural systems are of difficult quantification and there is a need for reliable data for a great number of elements and melt compositions.

In order to provide new insight of trace element mobilities, diffusion coefficients for those elements which profiles clearly outline a detectable flux were measured. A more exhaustive discussion is reported in the next chapter.

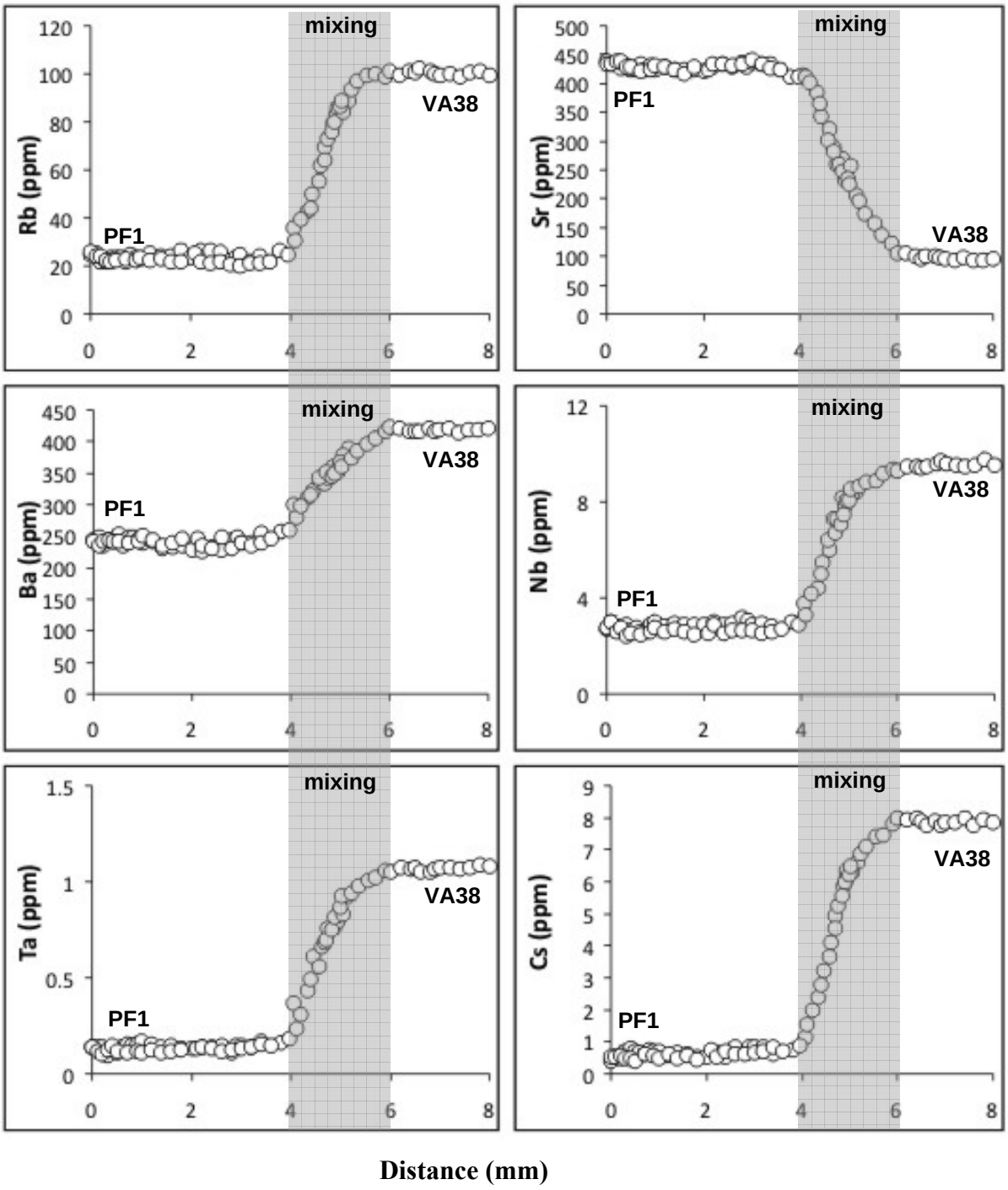


*Figure 4.4.2. Trace element variations with a perfect mixing rule.*

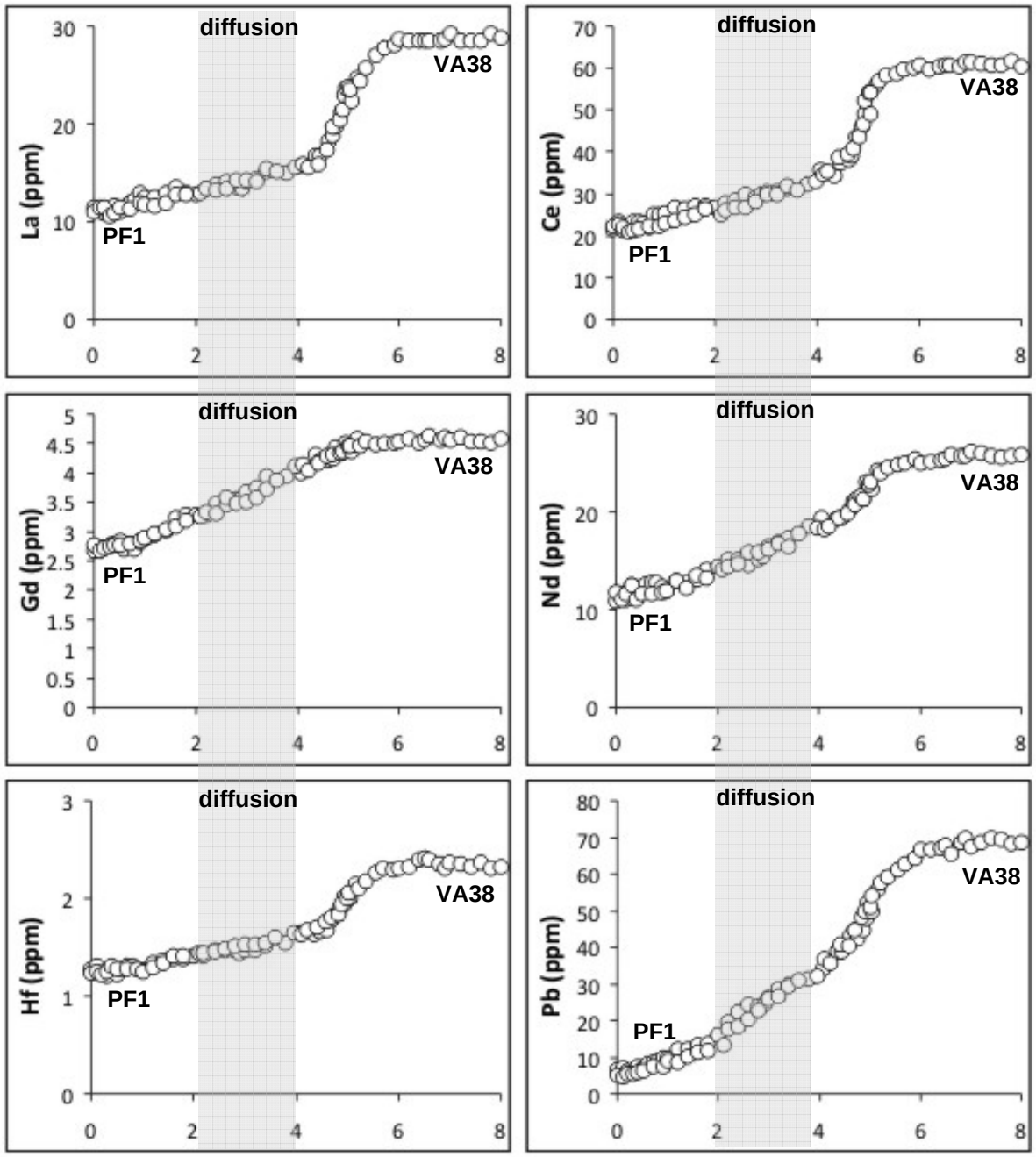


*Figure 4.4.3. Trace element diffusion in the basaltic reservoir.*

## 5 - Discussion and conclusions

The results of this research provide new insight into the mechanism of interaction between magmas and crustal material. However, in order to better understand how chemical modifications occur when two melts are contacting, the diffusion processes have to be take in consideration.

Diffusive transport in silicate melts is important in various magmatic processes. For example, chemical diffusion controls the degree of contamination of magmas by xenoliths and wall-rocks, and the rate of chemical and isotopic homogenization during magma mixing. As a consequence, diffusion could be one of the processes able to change the chemical composition of two interacting magmas, even if at limited extent.

Diffusion processes may be classified in the following categories: self-diffusion, tracer diffusion , and chemical diffusion.

In *self-diffusion*, no chemical concentration gradients are present, and the process is observed by labelling some of the atoms with radioactive or stable-isotope tracers.

In *tracer-diffusion*, a labelled tracer is introduced in the form of an isotope (usually radioactive) of a chemical element that is not otherwise present in the substance; the tracer amount is so small that no other appreciable concentration gradients are introduced.

In *chemical diffusion*, bulk chemical concentration gradients are present in the specimen. The motion of one element causes a counter flow of some other element and the flux of each component will depend on the gradients of all components in the system. While self and tracer diffusion are practically similar, a fundamental difference between these and chemical diffusion exists.

A phenomenological description of self and tracer diffusion, in one dimension, is by Fick's first law:

$$J_i = -D_i\left(\frac{dC_i}{dx}\right) \qquad (1)$$

Where J is the flux of tracer ($gcm^{-2}s^{-1}$), D is the diffusion coefficient ($cm^2s^{-1}$), C is the tracer concentration and x is the distance in the direction of diffusion; application of this equation to a volume element (when the

concentration changes with respect to time) and the requirement of conservation of mass, leads to the continuity equation (Fick's second law):

$$\frac{dC}{dt} = D\frac{d^2C}{dx^2} \qquad (2)$$

This equation considers D as constant, i.e is valid for self and tracer diffusion where the material properties are uniform.

Chemical diffusion in multi-component systems is described by Onsager's (1945) extension of Fick's laws:

$$J_i = -\sum_{j=1}^{n} D_{ij}\frac{dC_j}{dx} \qquad (3)$$

Where n is the number of independently variable components. The value of Dij will in general vary with composition. However, even with constant Dij, the flux of each component will depend on the gradients of all component in the system. This can easily lead to locally reversed concentration gradients, and the flux of a component i may be locally "uphill" (against its own concentration gradient!) because the sum of other terms may be greater and opposite in sign to the $i^{th}$ term.

Theoretically the Dij coefficient can be measured by determining concentration profiles of all the component in the system and solving the matrix for the vector equations equivalent to (3) (Gupta & Cooper, 1971). In practice, however it is very cumbersome and only treatment by Baker (1992) and Kress & Ghiorso (1994) have been attempted up now, even if their results are not still conclusive. This approach, however, is not valid if the coefficient are concentration-dependent.

A simplified approach in describing multi-component diffusion is to consider the system as pseudo binary: the flux of one component is simply viewed as being balanced by a counter flux in which all the other species are combined. An "Effective Binary Diffusion Coefficient" (EBDC) is thus obtained, which satisfies the Fick's equations provided: 1) all the concentration gradients are parallel to the same spatial direction and 2) the system is in a steady state or has no finite length in the direction of diffusion.

The above constraints ensure no curved path for Dij (bypassing the non-binary multi-component diffusion) and permit to consider the compositional path constant with time. If the element concentrations in the melt are not affected at the

end of the experimental assemblage, then the multi-component cross-effects can be neglected. Up now it is possible to evaluate the extent of chemical diffusion, only adopting simple models provided the elements migration occurs in absence of macroscopic movements of the two interacting fluids or in absence of heterogeneous reactions (bubbling or crystallization). Thus, the chemical profiles can be treated as a binary diffusion model for a semi-infinite volume with concentrations kept constant at one boundary. The solution of Fick's second law is:

$$C_i = C_o - erf\left(\frac{x}{2\sqrt{D_i t}}\right) \qquad (4)$$

where $C_i$ is the element concentration (wt%) at time t (s) and distance x (cm) from the interface, $C_o$ is the concentration at the origin (x=0), and $D_i$ is the diffusivity of the element.

Previous studies adopted the diffusion couples technique. This technique was applied to two coupled starting materials differing only in the concentrations of two elements (e.g. Na or K). The simplest experiments used one chemical homogeneous material doped with Na for half length of the capsule, while the other half was doped with K (Smith, 1974).

Watson (1976) and following works (Ryerson & Hess, 1978; Watson & Jurewicz, 1984; Johnston & Wyllie, 1988), evidenced a transient equilibrium state in diffusion experiments. The transient equilibrium is the process occurring in a zone in which motions of the elements toward two opposite sided compositions became so sluggish that does not cause chemical variations, as long as the structure-controlling species ($SiO_2$ and $Al_2O_3$) do not completely mix. The extent of transient equilibrium behaviour (i.e. the time require for the elements to escape from the transient zone) varies for each element, and is a function of the chemical composition of the liquid/s interested by diffusion. It is, in fact, influenced by the structural arrangement of the melt/s and strongly dictated by the ionic strength of each element.

Over the past 30 years, the problem of basalt contamination was faced by many authors interested on chemical processes occurring at the contact of molten basalt with different silicates (Yoder, 1973; Smith, 1974; Hofmann & Brown,

1976; Jambon & Carron, 1973; Watson, 1982; Watson & Jurewicz, 1984; Johnston & Willy; Van Der Laan & Wyllie, 1993; Kress & Ghiorso, 1994: Patino Duce, 1995). Main conclusions from these studies are here shortly reported: I) two interacting melts produce a reaction layer beyond of that fast diffusional elements can modify their compositions; II) only a limited exchange of elements occurs and the identity of two contiguous magmas of different composition may be maintained, at least for a short period (hours) (Yoder, 1973); III) detectable $SiO_2$ contamination can be expected from interaction between basalt and quartzose xenoliths (Watson, 1982); VI) a very limited $SiO_2$ diffusivity ($10^{-9}$ or $10^{-10}$ $cm^2/s$) compared to the alkalies has been detected at the basalt-feldspar interaction ($10^{-7}$ or $10^{-8}$ $cm^2/s$); V) in basalt-granite glass interactions, the diffusion profiles of less mobile elements are similar to that of Si, while alkalies diffusion is faster (Watson, 1982). All these results demonstrated that when crustal materials are partially melted by an underlying basaltic magmas, selective contamination of the basalt is indeed likely.

In PF1/VA38 experiments, an interaction layer develops between the two melts and in the basaltic domain, beyond the interaction layer, alkalies suffer great modifications, while the other component contents are virtually constant. Thus, provide us the opportunity to apply the Fick's second low solution for the diffusion into a semi-infinite medium from a surface at which the diffusant concentration is held constant. Estimated $D_{Na}$ and $D_K$ are reported in table 5.1. Even if, particular attempt was not adopted to discriminate the diffusional processes from the mixing phenomena (e.g. by checking the mixing extent with a run quenched immediately when the experimental temperature was reached), the obtained diffusion coefficients has been compared to those measured by authors, in basaltic compositions (table 5.2).

*Table 5.1. Calculated alkali diffusion coefficients.*

| Alkali | t (h) | D ($10^{-8}$ $cm^2/s$) | $D_{mean}$ ($10^{-8}$ $cm^2/s$) |
|---|---|---|---|
| Na | 1 | 40 | 39 |
| | 2 | 39 | |
| | 4 | 38 | |
| | 8 | 38 | |
| K | 1 | 13 | 12 |
| | 2 | 12 | |
| | 4 | 12 | |
| | 8 | 11 | |

*Table 5.2. Alkali diffusion coefficients from literature.*

| T (°C) | $D_{Na}$ ($10^{-8}$ $cm^2/s$) | $D_K$ ($10^{-8}$ $cm^2/s$) | Technique | Author (year) |
|---|---|---|---|---|
| 1300 | 200 | - | Tracer diffusion | Hoffman & Brown (1976) |
| 1300 | - | 100 | Chemical diffusion | Smith (1974) |
| 1300 | 1000 | - | Chemical diffusion | Watson (1982) |
| 1250 | 300 | 3 | Self diffusion | Watson & Jurewicz (1984) |
| 1200 | - | 18 | Chemical diffusion | Smith (1974) |
| 1200 | - | 50 | Chemical diffusion | Watson (1982) |
| 1000 | 10 | 6 | Tracer diffusion | Jambon& Carron (1973) |
| 950 | 4 | 2 | Tracer diffusion | Jambon& Carron (1973) |
| 850 | 2 | - | Tracer diffusion | Jambon& Carron (1973) |

In fig. 5.1, $D_{Na}$ and $D_K$ are plotted as a function of the experimental temperatures. Open and closed symbols are adopted to discriminate $D_{Na}$ and $D_K$, respectively, and different shapes are referred to the different experimental works: triangle, Smith (1974); square, Hoffman & Brown (1976); diamond, Jambon & Carron (1973); circle, Watson (1982) and Watson & Jurewicz (1984); star, present work.

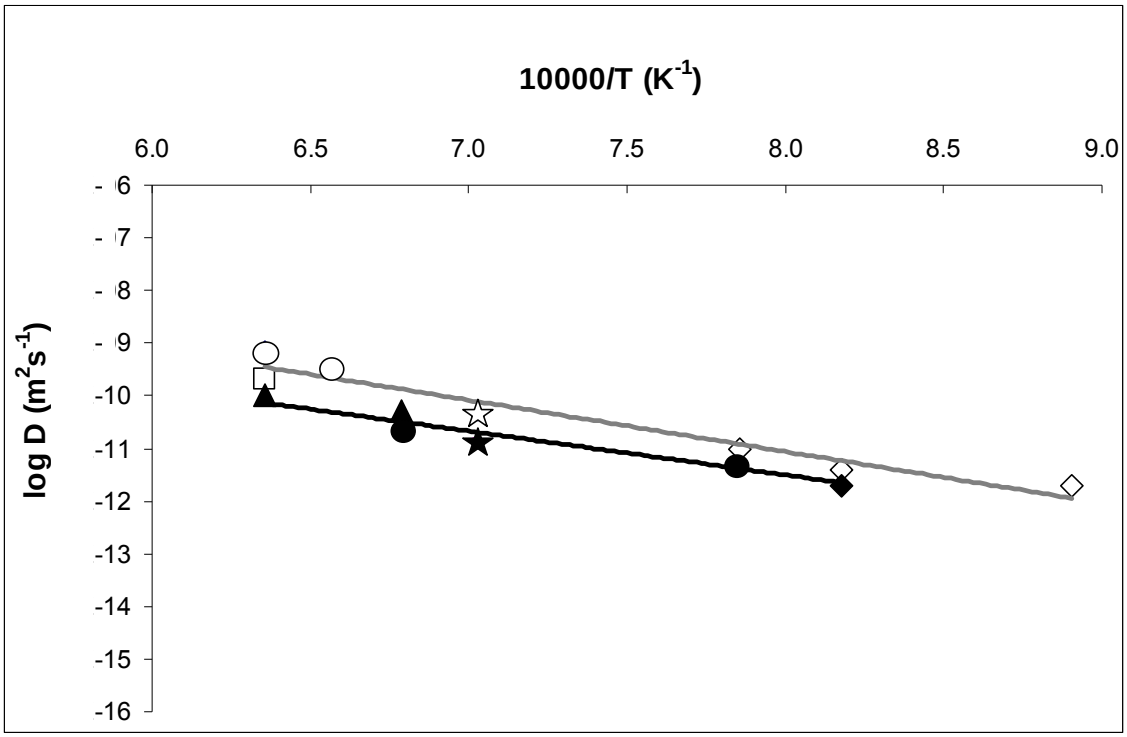


*Figure 5.1. $D_{Na}$ and $D_K$ variation with temperature.*

Even if, all these studies were conducted in variables P (0.001-0.1 GPa), T (850-1300 °C), and water contents, some considerations can be done.

1) Pressure is not one of the main parameter related to diffusional processes. In the previous studies, the pressure effect was seldom the principal focus of the work. Pressure influence was detailed investigated only by Baker (1990) that demonstrated a positive P and D correlation in metaluminous dacitic and rhyolitic melts interdiffusion experiments. However the effect of pressure on diffusivity is very small relating to the temperature one, and it could be considered negligible in a range from 0.001 to 0.1 GPa.

2) The amount of dissolved water affect the diffusion coefficient of melt components (Watson, 1979, 1981; Harrison & Watson, 1983, 1984; Baker, 1991; Mungall & Dingwell, 1994). The dependence of D with $H_2O$, is first exponential (below the 2 wt% amount of water), and then approximately linear. However, the increase of diffusivity is larger for a network-former cation such as $Si^{4+}$, than for a network-modifying like $Na^+$ or $K^+$ (Watson, 1994). If, the water content of a silicate melt is increased up to 4 wt%, then $D_{Si}$ increase up to 3 order of magnitude, whereas $D_{Na}$ does not change significantly (Richet et al., 2000).

According to these observations, it is plausible to consider negligible the water effect on the alkali diffusivity measured in glasses with less than 2 wt% of $H_2O$.

In fig. 5.1, alkali diffusion coefficients are well placed in the diagram, with a good correlation between D and T ($R^2$ is 0.92 and 0.90, for $D_{Na}$ and $D_K$ respectively). Two regression lines are reported in grey and black colour for $D_{Na}$ and $D_K$ respectively. A linear relation govern the two straight lines and it is described by the Arrhenius equation:

$D = D_0 \exp(-E_a/RT)$

where $D_0$ (derived from the intercept, when T is infinite) is expressed in $m^2s^{-1}$, Ea (proportional to the slope of the line) is the activation energy in $kJmol^{-1}$, R is the gas constant in $JK^{-1}mol^{-1}$ and T is the temperature in kelvin.

Equations calculated for the alkali diffusion in basaltic melt are:

$D_{Na} = 6 \times 10^{-4} \exp(-187\pm15/RT)$ (5)

$D_K = 1 \times 10^{-5} \exp(-159\pm16/RT)$ (6)

Diffusion coupling technique has been also adopted to calculate some trace element effective binary chemical diffusion coefficients during basalt/crust melt interactions.

Trace element diffusion in silicate melts were measured by authors in different ways (e.g. chemical, trace and self diffusion) both in hydrous and anhydrous systems. In previous works synthetic glasses were doped in few selected elements (Jambon, 1982; Lowry et al., 1982; LaTourette et al., 1996) and only recent studies report diffusion coefficients measured for more than 10 different elements at the same time (La Tourrette et al., 1996; Mungall et al. 1999; Koepe and Beherens; 2001). All these experiments were designed to calculate trace element diffusivities by coupling two halves of the same synthetic glass doped with different amounts of the investigated elements. Thus, in terms of major components, a single melt chemistry has been always adopted for all the experiments and therefore element diffusion occurred in the same compositional matrix. Until now, experimental data to better understand the influence of distinct interacting chemical matrixes on the trace element diffusivities have not been reported. Furthermore, literature data are of difficult comparison because the occurrence of few data and the sparse materials and the investigated experimental conditions. For example, the diffusivity of Yb, Ti, Zr and U in a basaltic melt was

measured for the first time only in 1996 by LaTourette et al.. However, one important result of these works was that addiction of water to silicate melt raises the trace element diffusion coefficients and lowers the activation energies. Elements with a low diffusivity in dry melts (e.g. Zr, Th) exhibit a greatest enhancement in hydrous conditions (Mungall and Dingwell, 1997 and references therein). Unfortunately, such variations make difficult to determine an Arrhenius relation for a unique system.

Here, we illustrate results of the first attempt to determine trace element diffusivities between two contacting natural compositions. The different interacting chemical matrixes and the simultaneously presence of at least 20 different trace elements, give us the possibility to investigate element diffusivity in a condition similar to natural. However, diffusion coefficients were calculated with reliable results only for such elements which showed a well appreciable chemical gradient and a defined diffusional profile between the contacting melts. D measurements were performed only in the basaltic layer due to 1) crustal chemistries variations with time; 2) appreciable trace element variations occurrence in the basaltic melt; 3) constant basalt chemistry in the PF1/MK72 runs and approaching a constant composition in the PF1/VA38 experiments.

Calculated diffusion coefficients from PF1/VA38 experiment are reported in table 5.3. The average values for REE and Y are, within the analytical errors, close to 1.23 $cm^2/s$. Comparison with literature data shows as Hf diffusivity is of the same order of magnitude of that calculated by Koepke & Behrens (2001) in synchrotron X-ray fluorescence. Yb, Nd, and U, overlap those of LaTourette et al. (1996), whereas Gd and Eu are in agreement with those calculated by Margaritz & Hofmann (1978). Comparisons reinforce the reliability of our estimations not only because are in agreement with literature data, but because as discussed below, some general trace element behaviours are respected during the diffusion process.

*Table 5.3. Calculated trace element diffusion coefficients in PF1/VA38 experiment.*

| Element | D ($10^{-7}$ $cm^2/s$) | σ |
|---|---|---|
| Y | 1.33 | 0.09 |
| La | 1.98 | 0.40 |
| Ce | 1.93 | 0.39 |
| Pr | 1.90 | 0.38 |
| Nd | 1.83 | 0.37 |
| Sm | 1.80 | 0.36 |
| Eu | 1.72 | 0.34 |
| Gd | 1.70 | 0.34 |
| Tb | 1.67 | 0.33 |
| Dy | 1.50 | 0.30 |
| Ho | 1.38 | 0.28 |
| Er | 1.30 | 0.26 |
| Tm | 1.20 | 0.24 |
| Yb | 1.11 | 0.22 |
| Lu | 1.10 | 0.22 |
| Hf | 0.36 | 0.03 |
| Pb | 6.61 | 0.46 |
| Th | 0.48 | 0.03 |
| U | 0.36 | 0.03 |

In PF1/MK72 run, diffusion process are not ruled by the chemical gradients between the two starting compositions. In fact, crystallization of plagioclase in the interaction layer modifies the original gradients, making the interacting composition the active counterpart at the contact with the basalt and replacing the MK72 melt in the diffusive process. Such exchange clearly results from our data which evidence a net flux toward PF1 (fig. 3.4.2) starting from the hybrid melt, where trace element amounts are enriched with respect to both starting compositions. In this case a "new apparent" diffusion coefficient can be estimated for elements which show a well recognizable diffusional profile. We call such diffusion coefficient new, because is related to melts different from the initials. To explain the anomalous enrichment in the hybrid melt, we infer that plagioclase crystallization, concentrates in the coexisting melt those elements incompatible in the mineral structure. Nevertheless, such consideration can not be invoked for Sr and at minor extent for Ba. Two justifications can be suggested: 1)

compatibility is reduced under kinetics driven conditions; 2) crystals in the growing stage speed up the drag capacity of compatible elements from the feeding melt. This can be sustained by the tail observed in the MK72 side only for such elements.

In table 5.4 calculated PF1/MK72 diffusion coefficients are reported. Values are one order of magnitude greater than in PF1/VA38 experiments and are not consistent with the chemical characters of the elements themselves.

*Table 5.4. Calculated trace element diffusion coefficients in PF1/MK72 experiment.*

| | **D** ($10^{-7}$ $cm^2/s$) | ± |
|---|---|---|
| La | 10 | 1.0 |
| Dy | 60 | 6.0 |
| Hf | 70 | 7.0 |
| Nb | 3 | 0.3 |
| Zr | 20 | 2.0 |
| Th | 8 | 0.8 |
| Cs | 10 | 1.0 |
| Rb | 10 | 1.0 |
| Sr | 8 | 0.8 |
| Ba | 10 | 1.0 |

Previous work, evidenced that the general effect of increasing atomic radius is to increase the activation energy for diffusion (Jambon, 1982; Koeple and Behrens, 2001). Smaller cation radius corresponds to higher values of the diffusion coefficient. However, element diffusivity depends on ionic radius and charge. For a given charge, diffusion coefficients generally decrease with increasing ionic radius. Such behaviour is not respected when elements with different charges are compared. An empirical relationship between logD and $Z^2/r$ (Z=charge and r=ionic radius), was proposed by Hoffman (1980). LaTourette et al. (1996) confirmed that smaller $Z^2/r$ ratios correspond to higher logD values and evidenced as the cation charge effect is double, compared to the ionic radius, in

reducing trace element diffusivity. In fig. 5.2, measured diffusion coefficients are plotted against the $Z^2/r$ ratios. In PF1/VA38 experiment variations are in agreement with the expected mobility even if two groups can be distinguished (closed circles). The same does not rule for the PF1/MK72 run (open circles). Some HFSE (Zr and Hf) have higher diffusion coefficients compared to LILE (Rb, Sr and Ba), while an "expected" lower diffusivity is observed for Nb. Such results denote that trace element behaviours must be revised when crystallization occurs in the interacting melts. They point out, as well, the necessity to deeply investigate the role of the interaction layer when melts with different chemical matrixes are put in contact.

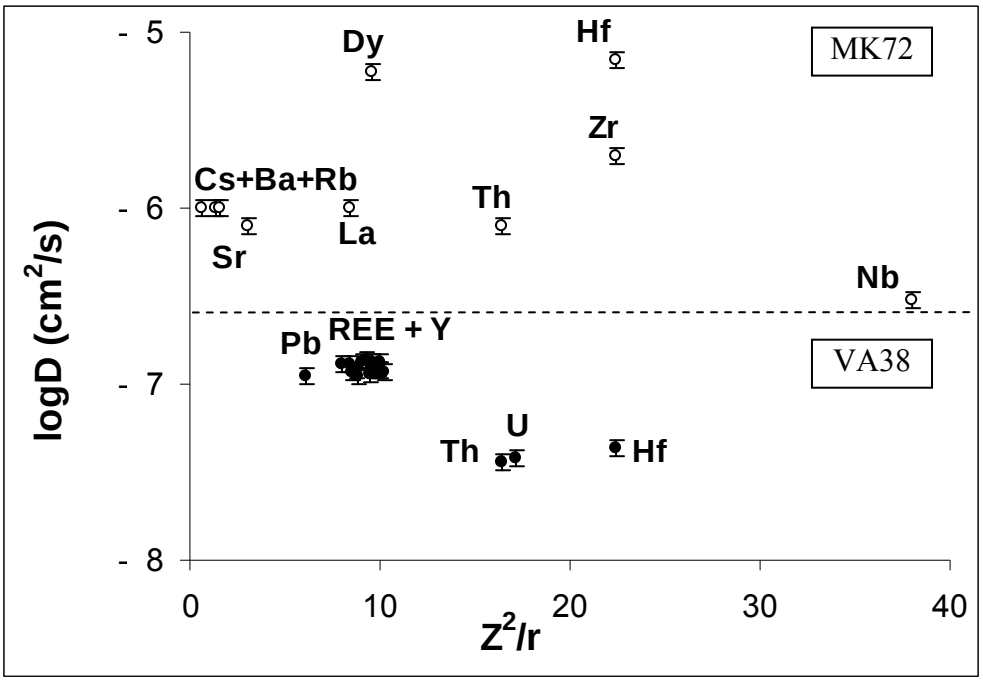


*Figure 5.2. Negative correlation of diffusion coefficients with cation $Z^2/r$ ratios. Cations ionic radii from Shannon (1976). Closed circle:PF1/VA38 run. Open circle: PF1/MK72 run.*

A "fanciful scenario" of magmatic contamination can be sketched adopting the obtained diffusion coefficients in the "unlucky case" in nature, conditions similar to the experimental ones are realized in persist for a long time. The interaction

will extend deeper toward the internal body of the basaltic batch, partially modifying its composition as reported in figure 5.3.

Calculation is simplified by assuming a statistical random movement of atoms with time (t) and linear distance (x). Considering that $x = r\sqrt{N}$, where r is the jump distance and N is the number of the atomic jumps in the glass structure. If a fixed jump rate (ν) is assumed, then $x \approx r\sqrt{\nu t}$; as it can be shown, $D \approx \nu r^2$ and substituting $x \approx \sqrt{Dt}$.

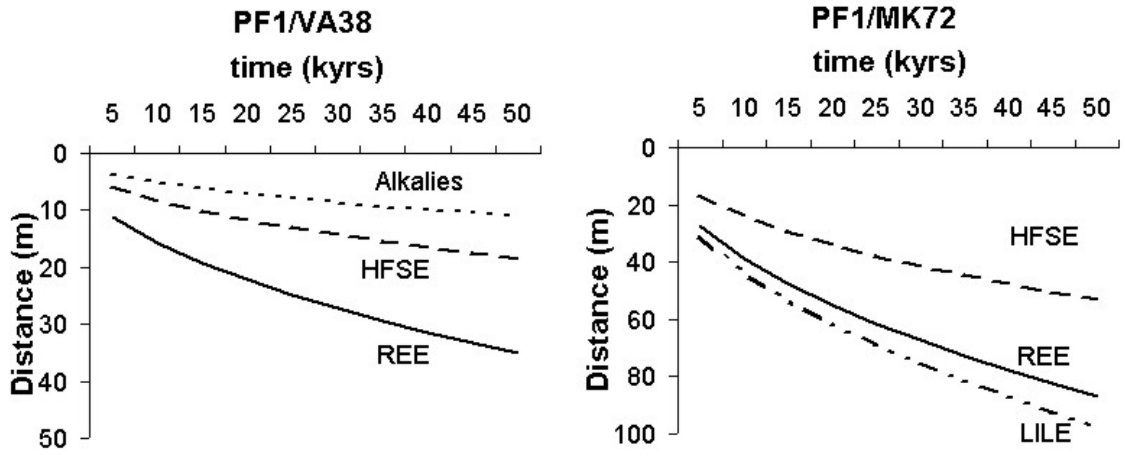


*Figure 5.3. Trace element contamination-rate.*

Not only the thickness of the zone interested by diffusion would change, but even the ratios of some elements will be affected when partial crystallization of the "engine" hybrid layer is considered. Clearly this figure is not sustainable for long term processes because crystallization in the basalt and the effect of the advancing solidification front, will add their imprinting to the entire process. It is not to be excluded, however, that diffusional processes can be at the base of noticeable mismatches when mass balances performed according to a Rayleigh model as well as a simple AFC are operated on different rock samples belonging to the same evolutive serie outcropping in a restricted areal region and emplaced in a short span of time.

## References


Alibert, C. & Carron, J.P. (1980). Donnees experimentales sur la diffusion des elements majeurs entre verres ou liquides de compositions basaltique, rhyolitique et phonolitique, entre 900 °C et 1300 °C, a pression ordinaire. Earth Planet. Sci. Lett., 47, 294-306.

Appel, P., Möller, A., Schenk, V. (1998). High-pressure granulite facies metamorphism in the Pan-African Belt of eastern Tanzania:P-T-t evidence against granulite formation by continent collision. J. of Metam. Geol., 16, 491-509.

Baker, D.R. (1990). Chemical interdiffusion of dacite and rhyolite: anhydrous measurements at 1 atm and 10 kbar, application of transition state theory, and diffusion in zoned magma chambers. Contr. Min. Petr., 104, 407-423.

Baker, D.R. (1991). Interdiffusion of hydrous dacitic and rhyolitic melts and the efficacy of rhyolite contamination by dacitic enclaves. Contr. Min. Petr., 106, 462-473.

Baker, D.R. (1992). Interdiffusion of geologic melts: calculations using transition state theory. Chem. Geol., 98, 11-21.

Baker, D.R. (1992). Tracer diffusion of network formers and multic-omponent diffusion in dacitic and rhyolitic melts. Geochim. Cosmochim. Acta, 56, 617-631.

Baker, D.R. & Watson E.B. (1988). Diffusion of major and trace elements in compositionally-complex Cl- and F-bearing silicate melts. J. Non-Cryst. Solids, 102, 62-70.

Beccaluva, L., Di Girolamo P., Serri, G. (1991). Petrogenesis and tectonic setting of the Roman volcanic province. Lithos, 26, 191-221.

Beccaluva, L., Macciotta, G., Siena, F., Zeda, O. (1989). Harzburgite-lherzolite xenoliths and clinopyroxene megacrysts of alkaline basic lavas from Sardinia. Chem. Geol., 77, 331-345.

Bohlen, S.R. (1984) Equilibria for precise pressure calibration and a friction less furnace assembly for the piston-cylinder apparatus. Neues Jahrbuch für Mineralogie Monatshefte, 9, 404–412.

Bowen, N.L. (1928) The evolution of igneous rocks. Princeton University Press, Princeton, NJ, 332 pp.

Carminati, E., Wortel, M.J.R., Meijer, P.Th., Sabadini, R. (1998). The two-stage opening of the western-central Mediterranean basins: a forward modelling test to a new evolutionary model. Earth Planet Sci. Lett., 160, 667-679.

Castorina, F., Stoppa F., Cundari, A., Barbieri, M. (2000). An enriched mantle source for Italy's melilitite-carbonatite association as inferred by its Nd-Sr isotope signature. Min. Mag., 64, 625-639.

Coolen, J.J. (1980). Chemical petrology of the Furua granulite complex, southern Tanzania. Geology, 1, 13.

Dallai, L, Freda, C., Gaeta, M. (2004). Oxygen isotope geochemistry of pyroclastic clinopyroxene monitors carbonate contributions to Roman-type ultrapotassic magmas. Contrib. Mineral. Petrol., 148, 247-263.

De Paolo, D.J. (1981). Trace element and isotopic effects of combined wall-rock assimilation and fractional crystallization. Earth Planet Sci. Lett., 53, 189-202.

Dixon, J.E., Stolper, E., Delaney, J.R. (1988). Infrared spectroscopic measurements of H2O and CO2 contents in Juan de Fuca Ridge basaltic glasses. Earth Planet. Sci. Lett., 90, 87-104.

Doglioni, C. (1991). A proposal for the kinematic modelling of W-dipping subduction: possible applications to the Tyrrhenian-Appennines system. Terra Nova, 3, 423-434.

Ellam, R.M., Hawkesworth, C.J., McDermott, F., (1990). Pb isotope data from late Proterozoic subduction-related rocks: implications for crust-mantle evolution. Chem. Geol., 83, 165-181.

Faccenna, C., Mattei, M., Funiciello, R., Jolivet, L. (1997). Styles of back-arc extension in the Central Mediterranean. Terra Nova , 9, 126-130.

Ferrari L. and Manetti P. (1993). Geodynamic framework of the Tyrrhenian volcanism: a review. Acta Volc., 3, 1-9.

Francalanci, L., Davies, G.R., Lustenmhower, W., Tommasini, S., Mason, P.R.D., Conticelli S. (2005). Intra-grain Sr Isotope Evidence for Crystal Recycling and Multiple Magma Reservoirs in the Recent Activity of Stromboli Volcano, Southern Italy. J. Petrol., 46, 1997-2021.

Freda, C., Baker, D.R., Ottolini, L. (2001). Reduction of water loss from gold-palladium capsules during piston-cylinder experiments by use of pyrophyllite powder. Amer. Min., 86, 234-237.

Freda, C., Gaeta, M., Karner, D.B., Marra, F., Renne, P.R., Taddeucci, J., Scarlato, P., Christensen, J.N., Dallai, L. (2006). Eruptive history and petrologic evolution of the Albano multiple maar (Alban Hills, Central Italy). Bull. Volc., 68, 567-591.

Frezzotti, M.L., Peccerillo, A., Bonelli, R. (2003). Magma ascent rates and depths of crustal magma reservoirs beneath the Aeolian volcanic arc (Italy): inferences from fluid and melt inclusions in xenoliths. In: Melt Inclusions in Volcanic Systems, B. De Vivo and R.J. Bodnar, edts., Elsevier, Amsterdam, 185-205.

Gaeta, M., Freda, C., Christensen, J.N., Dallai, L., Marra, F., Karner, D.B., Scarlato, P. (2006). Time-dependent geochemistry of clinopyroxene from Alban Hills (Central Italy): clues to source and evolution of ultrapotassic magmas. Lithos, 86, 330-346.

Gill, J.B. (1981). Andesites and Plate Tectonics. Springer, Berlin, 390.

Giordano, D, Mangiacapra, A., Potuzak, M., Russell, J.K., Romano, C., Dingwell, D.B., Di Muro, A. (2006). An expanded non-Arrhenian model for silicate melt viscosity: A treatment for metaluminous, peraluminous and peralkaline liquids. Chem. Geol., 229, 42-56, 2006.

Ghiorso, M.S. (1985). Chemical mass transfer in magmatic processes. I. Thermodynamic relations and numerical algorithms. Contrib Min. Petrol., 90, 107-120.

Ghiorso, M.S. & Carmichael, I.S.E. (1985). Chemical mass transfer in magmatic processes. II. Applications in equilibrium crystallization, fractionation and assimilation. Contrib. Min. Petrol., 90, 121-141.

Ghiorso, M.S. & Sack, R.O. (1995). Chemical Mass Transfer in Magmatic Processes. IV. A Revised and Internally Consistent Thermodynamic Model for the Interpolation and Extrapolation of Liquid-Solid Equilibria in Magmatic Systems at Elevated Temperatures and Pressures. Contr. Min. Petrol., 119, 197-212.

Gill, J.B. (1981): Andesites and Plate Tectonics. Springer, Berlin, 390.

Grove, T.L., Kinzler, R.J., Baker, M.B., Donnelly-Nolan, J.M., Lesher, C.E. (1988). Assimilation of granite by basaltic magma at Burnt Lava flow, Medicine Lake volcano, northern California. Contr. Min. Petr., 99, 320-343.

Gupta, P.K. & Cooper A.R., Jr (1971). The [D] matrix for multi-component diffusion. Physica, 54, 39-59.

Harrison, T.M. & Watson, E.B. (1983). Kinetics of zircon dissolution and zirconium diffusion in granitic melts of variable water content. Contr. Min. Petr., 84, 67-72.

Harrison, T.M. & Watson, E.B. (1984). The behavior of apatite during crustal anatexis: Equilibrium and kinetic considerations. Geochim. Cosmochim. Acta, 48, 1467-1477.

Hildreth W. & Moorbath S. (1988). Crustal contributions to arc magmatism in the Andes of Central Chile. Contr. Min. Petrol., 98, 455 - 489.

Hofmann, A.W. (1980). Diffusion in natural silicate melts: a critical review. In R. B. Hargraves, Ed., Physics of Magmatic Processes, Princeton University Press.

Hofmann, A.W. & Brown, L. (1976). Diffusion measurements using fast deuterons for in situ production of radioactive tracers. Carnegie Inst. Wash. Year Book, 75, 259-262.

Hudon, P., Baker, D.R., Toft, P.B. (1994). A high-temperature assembly for 1.91-cm (3/4-in.) piston-cylinder apparatus. Amer. Min., 79, 145-147.

Jambon, A. (1982). Tracer Diffusion in Rhyolitic Melts: experimental results for Na, K, Ca, Sr, Ba, Ce, Eu, to 1300 °C and a model of calculation. J. Geophys. Res., 87, 10797-10810

Jambon, A. & Carron, J. P. (1973). Étude expérimentale de la diffusion cationique dans un verre basaltique: alcalins et alcalinoterreux. Bull. Soc. Fr. Min. Crist., 101, 22-26.

Johnston, A.D. & Wyllie, P. J. (1988). Interaction of granite and basic magmas: experimental observations on contamination processes at 10 kbar with $H_2O$. Contr. Min. Petr., 98, 352-362.

Kawamoto, T. & Hirose K. (1994). Au-Pd Sample Containers of Melting Experiments on Iron and Water Bearing Systems. Europ. J. Min., 6, 381-385.

Koepke J. and Behrens H. (2001) Trace element diffusion in andesitic melts: an application of synchrotron X-ray fluorescence analysis. Geochim. Cosmochim. Acta 65, 1481-1498.

Koyaguchi T. (1989). Chemical gradient at diffusive interfaces in magma chambers. Contrib. Min. Petrol., 103, 143-152.

Kress, V.C. & Carmichael, I.S.E. (1988). Stoichiometry of the iron oxidation reaction in silicate melts. Amer. Min., 73, 1267-1274.

Kress, V.C. & Ghiorso, M.S. (1994). Multi-component diffusion in basaltic melts. Geochim. Cosmochim. Acta, 59, 313-324.

Kushiro, I. (1990). Partial melting of mantle wedge and evolution of island arc crust. J. Geophys. Res., 95, 15929–15939.

Lowry, R.K., Henderson, P., Nolan, J. (1982). Tracer diffusion of some alkali, alkaline-earth and transition element ions in basaltic and andesitic melt, and the implications concerning melt structure. Contr. Min. Petrol., 80, 254-261.

Lange, R.A. & Carmichael I.S.E. (1987). Densities of $Na_2O$-$K_2O$-CaO-MgO-FeO-$Fe_2O_3$-$Al_2O_3$-$TiO_2$-$SiO_2$ liquids: new measurements and derived partial molar properties. Geochim. Cosmochim. Acta, 53, 2195-2204.

LaVecchia G. & Stoppa F. (1996). The tectonic significance of Italian magmatism: an alternative view. Terra Nova, 8, 435-343.

LaTourette, T., Wasserburg, G.J., Fahey, A.J., (1996). Self diffusion o Mg, Ca, Ba, Nd, Yb, Ti, Zr and U in haplobasaltic melt. Geochim.Cosmochim.Acta, 60,1329–1340.

Lustrino, M., Melluso, L., Morra V. (2000). The role of lower continental crust and lithospheric mantle in the genesis of Plio-Pleistocene volcanic rocks from Sardinia (Italy). Earth Planet. Sci. Lett., 180, 259-270.

Margaritz, M. & Hofmann, A. W. (1978). Diffusion of Eu and Gd in basalt and obsidian. Geochim. Cosmochim. Acta 42, 847-858.

Misiti, V. 2004. Petrology of high-grade thermometamorphic rocks of Gennargentu (Sardinia, Italy). PhD Thesis, Università La Sapienza Roma.

Muhongo, S. & Lenoir, J.L. (1994). Pan-African granulite-facies metamorphism in the Mozambique Belt of Tanzania: U-Pb zircon geochronology. Journal of the Geological Society, London, 151, 343–347.

Mungall, J.E., Dingwell, D.B., Chaussidon, M. (1999). Chemical diffusivities of 18 trace elements in granitoid melts. Geochim. Cosmochim. Acta, 63, 2599-2610.

Mungall, J. & Dingwell, D.B. (1994). Effects of water content, temperature, and pressure on actinide tracer diffusion in melts of haplogranitic composition. Mineralogical Magazine, 58A, 636-637.

Mungall, J. & Dingwell, D.B. (1997). Actinide tracer diffusion in a haplogranitic melt. Geochim. Cosmochim. Acta, 61, 2237-2246.

Spear, F.S. & Cheney, J.T. (1989). A petrogenetic grid for pelitic schists in the system $SiO_2$ - $Al_2O_3$ - FeO - MgO - $K_2O$ - $H_2O$. Contr. Min. Petr., 101, 149-164.

Nakamura, E. & Kushiro, I. (1988). Trace element diffusion in jadeite and diopside melts at high pressures and its geochemical implication, Geochim. Cosmochim. Acta, 62, 3151-3160.

Onsager, L. (1945). The distribution of energy in turbulence. Phys. Rev., 68, 286.

Patiño Douce, A.E. (1995). Experimental generation of hybrid silicic melts by reaction of high-Al basalt with metamorphic rocks. J. Geophys. Res, 100, 623-639.

Peccerillo, A., Poli, G., Serri G. (1988). Petrogenesis of orenditic and kamafugitic rocks from Central Italy. Canad. Min., 26, 45-65.

Peccerillo, A. (1999). Multiple mantle metasomatism in central-southern Italy: geochemical effects, timing and geodynamic implications. Geology, 27, 315-318.

Peccerillo, A., Dallai, L., Frezzotti, M.L., Kempton P.D. (2004). Sr-Nd-Pb-O isotopic evidence for decreasing crustal contamination with ongoing magma evolution at Alicudi volcano (Aeolian arc, Italy): implications for style of magma-crust interaction and for mantle source compositions. Lithos, 78, 217-233.

Peccerillo A. & Lustrino M. (2005). Compositional variations of the Plio-Quaternary magmatism in the Circum-Tyrrhenian area: Deep- vs. shallow-mantle processes. In: Foulger G.R., Nathland G.H., Presnall D.C., Anderson D.L. (editors), Plates, plumes, and paradigms. Geol. Soc. Amer., 388, 421-434.

Peccerillo, A. (2005). Plio-Quaternary Volcanism in Italy: Petrology, Geochemistry, Geodynamics. Springer-Verlag.

Patiño Douce, A.E. (1995). Experimental generation of hybrid silicic melts by reaction of high-Al basalt with metamorphic rocks. J. Geophys. Res., 100, 623-639.

Rutter, M. J. (1987). Evidence for crustal assimilation by turbulently convening, mafic alkaline magmas: geochemistry of mantle xenoliths-bearing lavas from Northern Sardinia. Journal of Volcanology and Geothermal Research, 32, 343–354.

Santo, A.P. , Jacobsen S.B., Baker J. (2004). Evolution and genesis of calc-alkaline magmas at Filicudi Volcano, Aeolian Arc (Southern Tyrrhenian Sea, Italy). Lithos, 72, 73-96.

Serri, G., Innocenti, F. and Manetti, P. (1993). Geochemical and petrological evidence of the subduction of delaminated Adriatic continental litosphere in the genesis of the Neogene-Quaternary magmatism of central Italy.

Shannon, R.D. (1976). Revised effective ionic radii and systematic studies of interatomic distances halides and chalcogenides. Acta Cryst. A32, 751-767.

Smith, H.D. (1974). An Experimental Study of the Diffusion of Na, K, and Rb in Magmatic Silicate Liquids. Ph.D. Dissertation, University of Oregon.

Spear, F.S. & Cheney, J.T. (1989). A petrogenetic grid for pelitic schists in the system $SiO_2$ - $Al_2O_3$ - FeO - MgO - $K_2O$ - $H_2O$. Contr. Min. Petr., 101, 149-164.

Richet, P., Whittington, A., Holtz, F., Behrens, H., Ohlhorst, S., Wilke M. (2000). Water and the density of silicate glasses. Contr. Min. Petr., 138, 337-347.

Ryerson, F.J. & Hess, P.E. (1978). Implications of liquid-liquid distribution coefficients to mineral-liquid partitioning. Geochim. Cosmochim. Acta, 42, 921-932.

Taylor, H.P., JR (1980). The effects of assimilation on $^{18}O/^{16}O$ and $^{87}Sr/^{86}Sr$ systematics in igneous rocks. Earth Plan. Sci. Lett., 47, 243-254.

Van Achterbergh E. Ryan C. G. Griffin W. L. (1999). GLITTER: On-line interactive data reduction for the laser ablation ICP-MS microprobe. In: Proceedings of the 9$^{th}$ V.M. Goldschmidt Conference, Cambridge, Massachusetts, pp. 305-306.

Van der Laan, S.R. & Wyllie, P.J. (1993). Experimental interaction of granitic and basaltic magma and implications for mafic enclaves. J. Petrol., 34, 491-517.

Watson, E.B. (1976). Two-liquid partition coefficients: Experimental data and geochemical implications. Contr. Min. Petr., 56, 119-134.

Watson, E.B. (1979). Diffusion of cesium ions in $H_2O$-saturated granitic melt. Science 205, 1259-1260.

Watson, E.B. (1981). Diffusion in magmas at depth in the Earth: The effects of pressure and dissolved $H_2O$. Earth Plan. Sci. Lett., 52, 291-301.

Watson, E.B. (1982). Basalt contamination by continental crust: Some experiments and models. Contr. Min. Petr., 80, 73-87.

Watson, E.B. (1994). Diffusion in volatile-bearing magmas. In: Volatiles in Magmas, 371-411, (Reviews in Mineralogy, vol. 30, M.R. Carroll and J.R. Holloway, Eds.), Mineralogical Society of America, Washington D.C..

Watson, E.B. & Baker, D.R. (1991). Chemical diffusion in magmas: An overview of experimental results and geochemical implications. In: Advances in Physical Geochemistry, vol. 6, ed. by I. Kushiro and L. Perchuk, Springer Verlag, New York, 120-151.

Watson, E.B. & Jurewicz S.R. (1984). Behavior of alkalies during diffusive interaction of granitic xenoliths with basaltic magma. J. Geol., 92, 121-131.

Wyllie P.J., Carroll M.R., Johnston, A.D. Rutter, M.J., Sekine T. and Van Der Laan S.R., (1989). Interaction among magmas and rocks in subduction zone regiona: experimental studies from slub to mantle to crust. Eur J. Min., 1, 165-179.

Yoder, H.S. (1973). Contemporaneous basaltic and rhyolitic magmas. Amer. Min., 58, 153-171.